Response to Reviewer letter

Olesya Yakovchuk Jan Maik Wissing

August 13, 2019

Manuscript Title: Magnetic local time asymmetries in precipitating and trapped electron and proton populations with and without substorm activity
https://www.ann-geophys-discuss.net/angeo-2019-49
https://doi.org/10.5194/angeo-2019-49-RC1

Annotation

We would like to thank the reviewers for fruitful comments as they draw out attention to aspects that can be (better) answered by the used methods but somehow were off our radar.

As a couple of figures have been added (and one table has been replaced) we would like to note that the references in this reply belong to the old numbering.

Additionally we ereased the section about low latitudes since we noticed that the different longitudes contribute very unevenly to the MLT bins here. In case that reviewers' comments to that section have been answered before, we included the answers. Further explanation is given in a spectial section that reads:

1. Why is the SAA not evenly smeared out over all longitudes?

If we would take a look at the footpoints of a solar-synchronous satellite in local time we would see that it always crosses a particular latitude e.g. the equator at one particular local time in ascending mode (and another, at the equator 12 hours later, in descending mode). At high latitudes it crosses 12 local time zones on a few latitudes, but still, the next orbit will exactly match the first (except if the orbit moves, which also happens to the POES/METOP satellites, but on longer time scales). Looking at the footpoints of the same satellite in MLT changes quite a bit. Given that the MLT zones are based on magnetic latitude and the magnetic poles being shifted, it means that the MLT-footpoints especially in high latitudes differ significantly from one orbit to the next. Due to the POES inclination of 98.5 degrees the satellite may at maximum reach the northern magnetic pole. The southern magnetic pole however, may not only be reached but even passed.

Thus there are two options how the MLT during an orbit may develop in the southern hemisphere: If the satellite's longitude is far from the magnetic pole the orbit will not pass the magnetic pole and the MLT will gradually increase by 12 hours till it reaches the equator in ascending mode again. Let us call this "ascending MLT". In the other case ("descending MLT"), the southern magnetic pole will be passed and the magnetic local time zones will be flown through in the opposite direction, decreasing MLT by 12 hours till reaching the equator in ascending mode again. Since the southern magnetic pole is somewhat south of Australia a significant fraction of the orbits passing it will cross the SAA in descending mode (but not in ascending mode). The opposite is true for the ascending MLT path, which includes a significant fraction of orbits that pass the SAA in ascending mode.

In case multiple satellite are used this does not affect high latitudes, but in low latitudes the situation is different. Since the satellites are crossing the equator at two specific local times (for ascending and descending mode, being just slightly broader in MLT), MLT coverage at the equator is limited to these points. They however may be reached in ascending mode (or left in descending mode) by ascending or descending MLT paths. In Fig. 1, top right (or bottom right) the equator is crossed at six different smeared out MLTs. While the ones on the left (13, 17 -two satellites- and 21 MLT) represent the descending mode, the ones on the right (1, 5 and 9 MLT) are in ascending mode.

The ascending MLT path now connects e.g. the low flux right edge of the 21 MLT equatorial crossing with the high flux (SAA) left edge of the 9 MLT equatorial crossing. The descending MLT path on the other side connects e.g. the high flux (SAA) left edge of the 21 MLT equatorial crossing with the low flux right edge of the 9 MLT equatorial crossing.

In sum the ascending and descending MLT paths cause the left edge of an equatorial crossing to be affected by the SAA, while the right edge is not. Any MLT analysis of low latitudes based on POES/MEPED will suffer from the fact that the longitudes contribute very unevenly to the MLT zones. This hampers a flux analysis in low latitudes. In high latitudes however this effects gets counterbalanced by broader MLT coverage and multiple satellites.

Reviewer 1 (Comments)

The paper uses POES and METOP data to evaluate how the precipitation of protons and electrons varies with magnetic local time during both isolated substorms and in the absence of substorm activity. Data collected during the declining phase of cycle 23 has been used, and measurements from multiple energy channels evaluated. Overall this is an interesting piece of work and generally well written. The introduction and motivation in particular is very well thought out.

1. Comment

My major concern for the paper is that one of the authors main results, the Kp (or lack of) dependence of proton and electron precipitation, is discussed in the abstract as well as the summary section, but any figure actually showing this has been omitted from the paper. While an indication is given in table 2, this is difficult to assimilate and results considering different Kp bins need to be presented as a figure for this result to be claimed.

Reply: *The reviewer is right, that table 2 is just an "indication" of the Kp dependency that we noticed. However, it already pointed out what we now elaborated in more detail. As all channels and various Kp level had to be analyzed, it was now necessary to write an automated auroral oval detection algorithm for APEX 110 km latitude or MLT locations of the auroral oval or its flux maximum and minimum. The routine determines the maximum flux for each MLT-bin within the typical auroral latitude range. This results in a preliminary auroral oval. Then the latitudinal differences between MLT-predecessor and successor are determined and in case of large outliers a point is assumed to be a spike in the data and replaced by the next biggest flux-bin in that MLT zone. In case that more than 7 points have to be replaced for a auroral oval the according channel-Kp set is neglected. In sum this ends up in a well-working detection algorithm for the auroral oval and allows us to find its minimum and maximum flux, or their ratio. A sample output is given in the following figure.*

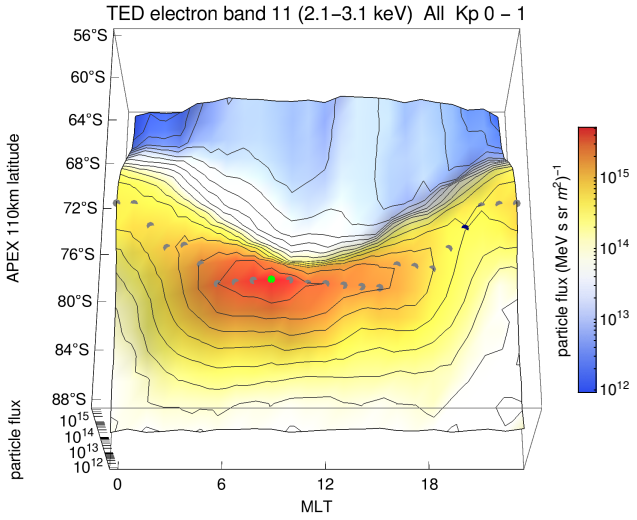

The gray dots represent the position of the auroral oval. The green (9 MLT) and black (20 MLT) dots indicate maximum and minimum of the auroral oval, respectively. All locations have been cross-checked manually.

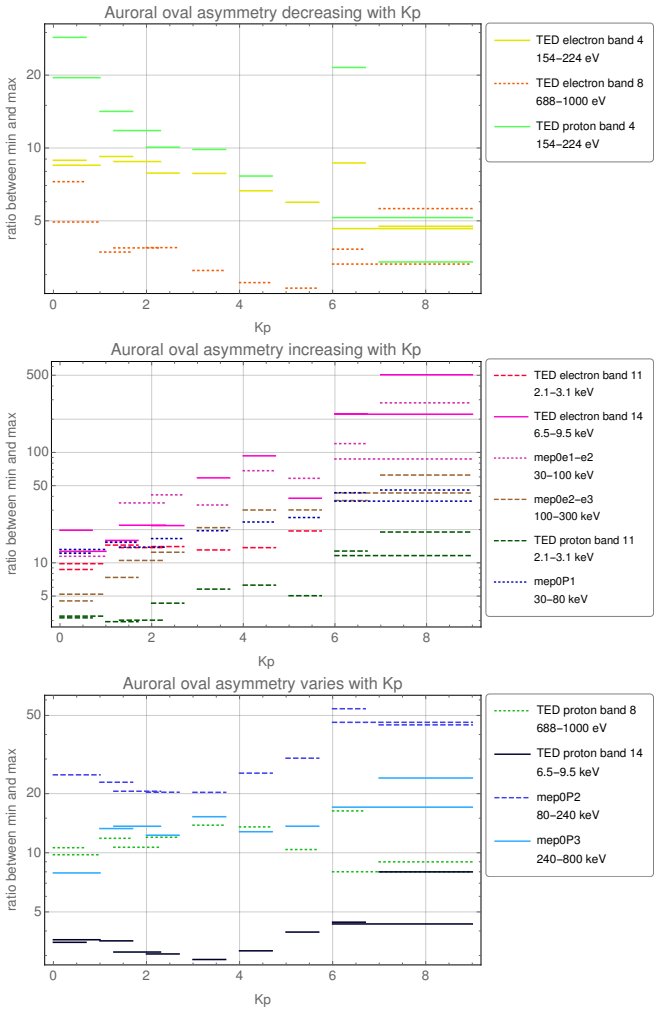

The next figure is based on these findings and presents the ratio between maximum and minimum auroral oval flux (or in other words the asymmetry of the oval) depending on Kp-level for every channel separately. Actually the channels have been grouped by their Kp dependency. The upper panel shows the 2 lowest electron channels and the lowest proton channel which all have a declining flux asymmetry with increasing Kp. The 6-6.7 Kp-bin is enhanced here, but we should keep in mind that this levels are occurring rarely and may suffer from bad statistics.

The middle panel shows all particle channels that have an increasing flux asymmetry with Kp, as they are: all remaining electron channels and the proton channels TED band 11 and mep0P1.

The lowest panel gives the flux asymmetry dependencies of the remaining proton channels that are less distinct. It seems that there is a domain change at about 3.3 Kp, since the asymmetry of TED proton band 14 and mep0P2 has a negative correlation below 3.3 and a positive one above. For the channels TED proton band 8 and mep0P3 the relationship is opposite.

All these findings are based on the whole period including all (no-) substorm conditions.

Another aspect that was mentioned in table 2 is how the asymmetry depends on substorms. The next figure presents this relation in more detail. Since an 8 year period does not contain enough values for substorms in rare Kp-levels we neglected the Kp-level here and compared isolated substorm to no-substorm periods.

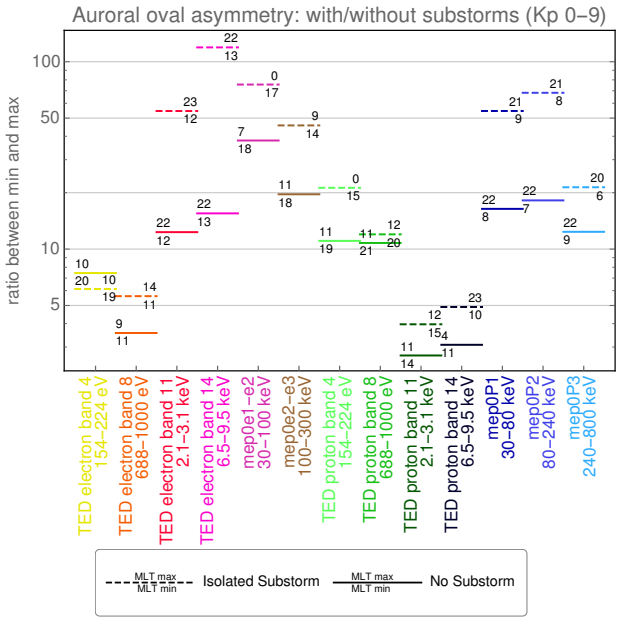

Except for TED electron band 4 (where there is no significant difference between substorm and no-substorm periods) all other channels have an increased auroral oval asymmetry during isolated substorms. The numbers above and below the marked flux ratio indicate the MLT location of the minimum (below) and maximum (above). We can identify that the maximum flux during a substorm shifts to the midnight sector (if not already there in no-substorm periods) e.g. for mep0e1-e2, TED proton band 4 and 14.

For TED electron band 4 and 8 (as well as TED proton band 8 and 11) the substorm enhancement is also seen in the night sector, but it does not overshoot the dayside flux (see Figures 2 and 3), while the substorm enhancement in the night-sector of mep0e2-e3 is in the same order as the 9–12 MLT flux.

The asymmetry in both, the electron and the proton spectrum shows a local minimum in middle TED channels (TED electron band 8 and proton band 11) as well as a local maximum at higher energies (TED electron band 14 or mep0e1-e2 for electron and mep0P1 or mep0P2 for protons). At even higher energies the asymmetry declines again.

This information has been added to the paper. Sections have been restructured accordingly. Given that the new

figures are more detailed than the previous table, the table will be omitted.

2. Comment

Line 19, section 1, discusses how the SML index was used to define the substorm onsets. While the reviewer agrees that SML is a good choice to define substorm onsets, perhaps the authors could elaborate on why SML was used instead of the AE index as in the Reeves et al., 2003 study.

Reply: *The link between AE and SML now is explained in more detail. The paragraph now reads: The occurrence of substorms depends on the orientation of the interplanetary magnetic field (Reeves et al., 2003). As shown in Reeves et al. (2003) these external solar wind parameters subsequently impact the magnetic field on the ground and are represented in the Auroral Electrojet (AE) index. Auroral Electrojet indices AE=AU-AL are a good proxy of the global auroral power, where AU and AL are the upper and lower components of AE, which means the largest and smallest values of the H component among 12 magnetic stations (Davis und Sugiura, 1966). AU represents the strength of the eastward electrojet, while AL represents the westward electrojet. Consequently AL seems to be the index which best corresponds to westward intensification of the auroral current aka substorm activity. Prior to substorm onset, AL index is typically small in magnitude, with the contributing station near dawn, whereas during substorm onset, the station contributing to the lower envelope is usually in the dusk sector under the auroral expansion. However, due to the limited spatial coverage of the 12 magnetometer stations the auroral expansion can be missed, which means that this index does not always reflect the onset (Gjerloev et al., 2004). The use of SuperMAG SML, an index derived likewise to the AE but based on all available magnetometer stations (typically more than 100) at these latitudes, considerably improves the detection of substorm onsets (Newell und Gjerloev, 2011). Thus we use the SML index in this study to define substorm onsets.*

3. Comment

In section 3, line 11-12 reads "the SAA allows energetic particles in the radiation belt to reach altitudes low enough to be reached by the satellites orbit". Considering that the authors are solely using the T0 flux measured by POES and METOP, Figure 1 in Rodger et al. (2010) would suggest that, even over the SAA, the T0 measured flux is still precipitating.

Reply: *Comparing Figure 1 in Rodger et al. (2010) to the upper panel of our Fig. 1 (in geographic coordinates) we can see that the SAA region (between 280 and 360 degrees East and -45 to 0 degrees North) covers a mix of all populations. The central part of the SAA is even located in the yellow area labled with "trapped+drift loss cone+bounce loss cone". In so far we disagree with the reviewer and conclude that the T0 flux measured in the SAA is not precipitating in total since it also contains a fraction of the trapped particles. As the following sentence reads "Thus the high flux values are not necessarily connected to high particle precipitation." we already tried to mention that. However, to point that out, we now added the following sentence: "According to Rodger et al. (2010: Fig. 1) the particle population in the SAA consists of particles precipitating in bounce and drift loss cone as well as trapped particles."*

4. Comment

In Figures 2, 3, and 4, as well as in the text, could the different energy channels be referred to by the energy range covered rather than the channel name? This would make the results easier to interpret without constantly flicking back to table 1.

Reply: *We agree with the reviewer that it might be helpful to give the energy ranges in every figure. However there are some caveats about the energy ranges that need to be mentioned: a) Some channels suffer from degradation. This mostly holds for the MEPED proton channels and is a result of structural defects caused by the impinging particles. On the long run it causes an energy shift (to higher particles energies) since less electron-hole pairs are produced per deposited particle energy. Consequently the mentioned energy ranges are nominal ranges. Further details on degradation of the MEPED channels can be found in e.g. Asikainen et al. (2012). b) For at least one channel the energy range seems to be doubtful as NOAA describes the same detectors in two technical documents with divergent ranges for mep0P2: 80–240 keV in (Evans und Greer, 2006) and the same channel in Green (2013): 80–250 keV. The electron channels also have different ranges as Green (2013) lacks an upper threshold energy. But since we subtract the electron channels in order to get differential channels this does not matter in our case anyway.*
We added the nominal energy range to all figures and added a note about the possible degradation.

5. Comment

When discussing figure 2 in section 4, point c and d mention that the noon sector flux decreases during a substorm. Could the authors speculate on why this is?

Reply: *We added the following information: "The noon sector flux decreases most probably because dayside*

particle precipitation occurs often during northward orientated IMF which is not usual for substorms."

6. Comment

When discussing Figure 3, the first point claims that protons also show an equatorial movement of the main precipitation zone with increasing particle energy. More direction to this in the figure is required here for the reader as I do not see this.

Reply: *The following figure presents the dependency of the latitude of the main precipitation zone to the particle energy.*

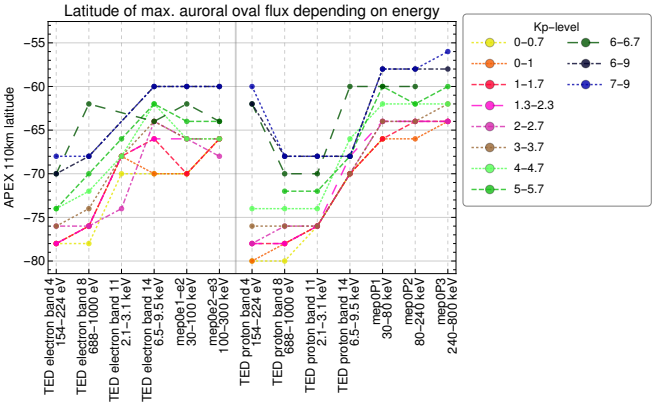

The figure has been derived by the auroral oval determination method discussed before and displays the latitude of maximum auroral oval flux. Except for some outliers, most of them belonging to TED proton band 4 during high Kp levels (> 6), the graphs show a clear equatorial dislocation with increasing energy. The 110 km APEX latitudinal range at a specific Kp-level is about 10° for electrons and 12-16° for protons. This dislocation however appears to be stepwise: TED electron band 4 and 8 are on the same latitude as well as TED electron band 14, mep0e1-e2 and mep0e2-e3 share the same latitude. For protons TED proton band 4, 8 and 11 are on one latitude and the higher particle energies mep0P1 and mep0P2 are colocated. This implies that these particles origin from the same souce region.
Every color graph represents the spectral location of the main precipitation zone for a certain Kp-range. Thus we can infer that increased geomagnetic disturbance (high Kp-values) causes a dislocation of up to about 8° towards the equator.
Concerning the outliers in TED proton band 4, for low Kp-values there is a clear flux maximum at noon, which is located at rather high latitudes (compare Fig. 2). At high Kp, the MLT asymmetry declines and then flips. Consequently the maximum flux for high Kp-levels is not in the day-sector and thus at significantly lower latitudes. This information has been added to the paper.

7. Comment

The second point made when discussing Figure 3 was that there is a second auroral oval. This is then stated to be an artefact of the MLT binning. Could the authors add further explanation to justify this here?

Reply: *We added a figure tha shows the APEX latitude and longitude. This figure nicely shows that the double auroral structure is on the same latitude as the drift loss cone. Also further explanation has been added. The following information now is included: "Figure 1 shows the TED proton band 11 in geographic coordinates (top row) and modified APEX 110 km coordinates (bottom row). The left column shows latitude against longitude while the right column shows latitude against MLT. No selection according to Kp-level or substorm intensity has been made, while all available data from METOP 2 and POES 15, 16, 17 and 18 for the years 2001–2008 has been included. This allows a spatial resolution of 3.75 degrees longitude (or 15 min MLT). Please note that latter figures show a reduced longitudinal resolution of 15 degrees (or 1 h MLT) only to avoid statistical noise in e.g isolated substorms periods."*
and
"Figure 1 (top, right) shows the same data on a geographic latitude vs. MLT grid. As the auroral oval is not visible as an oval any more but mixes up local time differences and the latitudinal variations that can already be seen in Fig. 1 (top, left)."
and
"Switching to magnetic modified APEX 110 km coordinates (see Fig 1, bottom, left) straightens the auroral oval and mostly removes the longitudinal dependence except for the SAA and the drift loss cone in the South of the SAA. Consequently we can replace the APEX longitude by MLT (see Fig. 1, bottom, right). Features that depend on magnetic local time now become visible and the auroral oval itself does not show a hemispheric dependence. The SAA and the drift loss cone, however, are now smeared out and still produce a hemispheric asymmetry. The drift loss cone that is located at a distinct modified APEX 110 km longitudinal range even appears as an double auroral structure at the same latitude but covering all longitudes. Which of course is an artifact of this kind of MLT binning."
In addition several references to the figure have been updated.

8. Comment

In the text, table 3 is not discussed or explained. Perhaps it is not needed? Otherwise the relevance needs to be discussed.

Reply: *The table is now referenced in the text.*

Typo

Additionally, there are a number of typographical errors in the manuscript:

Page 4, line 3: "furtunately",
Reply: *Corrected.*

Typo

Page 4, line 15: "trapped particles in low altitudes" should be "at low altitudes".

Reply: *Assuming that latitudes are meant we corrected the wrong preposition throughout the manuscript.*

Typo

Page 4, Line 25: "mainly located in about 110 km altitude" should be "at about 110 km...".

Reply: *Corrected.*

Typo

Page 4, Line 34: you have not defined the QD acronym - please write out quasi-dipole.

Reply: *The acronym has been added were the quasi-dipole system is introduced.*

Typo

Spelling of "avoid" throughout the manuscript is wrong.

Reply: *Corrected.*

Typo

Page 5, line 20: "independend".

Reply: *Corrected to "independent".*

Typo

Page 6, line 29: "Substorm depended precipitation..."

Reply: *Corrected.*

Reviewer 2 (Comments)

(We reordered the reviewer's comments to allow more structured answering.)

The paper describes electron and proton differential number flux $1/(m^2$-s-sr-MeV- according to the figure labels) measured in various energy channels by detectors on POES and METOP from 2001-2008 in the radial direction away from Earth for electrons and 9 degrees from that in protons. It presents the results of these by field line mapped latitude at 110 km altitude and by magnetic local time (MLT) for non-sub-storm times and isolated sub-storms. It also makes mention of comparisons to geomagnetic activity (Kp), but does not present any data in this regard. The data in the paper could have potential contributions to the field with additional work and resubmission.

At a very minimum these two major issues need to be addressed: the data and results need to be presented within the proper context (a useful review of the TED energy range precipitation is in by Frey, 2007), and a more precise description of what is presented/covered in the paper is required.

Until the paper is reworked into the proper context, it is difficult to determine whether the conclusions are significant (currently they are not), how important the contribution is, or if the length of the paper is adequate. The language is mostly fluent, but does need to be made more precise in ways, as mentioned. The figures are of adequate size, although the text in them is too small in some cases. The presentation is clear and organized, although missing the context for appropriate organization.

1. Comment

The data itself is a contribution to the field providing the same type of measurements and analysis over a wide energy range for both electrons and protons. However, the difference in scales for the different channels and the substantial difference in energy widths of the channels makes inter-comparison between the channels difficult other than relative locations of peaks and troughs and differentials, which are the focus of the paper results. Multiplying by the geometric mean of the channel energy ranges and dividing by the channel energy width would give a reasonable proxy for energy flux, which could be put on the same scale and would allow direct comparison of levels between the energy channels, which would add to the contribution from the presentation of the data.

Reply: *We agree with the reviewer that dividing the particle flux by the channels' energy range (resulting in a so called "differential flux" given in $1/(m^2\,s\,sr\,MeV)$, which we are using in the paper) and multiplying it with the mean kinetic energy of a particle detected in those channels would result in values that are closer together than the differential flux itself. However, as acceleration mechanisms are different, we do not see that "closer together" is equivalent to "more comparable". Our intention for the inter-comparison is two-fold: First we are interested in asymmetries in the main precipitation zone, the auroral oval. Using the minimum flux in the auroral*

oval as reference allows us to easily identify and quantify these asymmetries by color and in so far it sounds reasonable for us. Second, the differential flux is needed when transposing the particle precipitation into atmospheric ionization. This is not part of this paper, but since a later paper about atmospheric ionization will refer to these asymmetries it might be a good idea to have them in the correct format already.

We now added "All particle count rates have been converted into differential flux by dividing the energy range and a geometric factor has been applied as suggested in Evans und Greer (2006)." to avoid any misinterpretation. Also the paragraph about satellite data has been restructured.

2. Comment

The data would be a contribution (and could be improved as indicated), but a good amount of additional is required to other facets of the paper. In particular, there are two major components that need to be significantly improved. One is the need to put the data in appropriate context of previous work, empirical and physical theories. The results also would need to be appropriately put into context. The second is a loose use of language in important ways that causes misrepresentation of the data and focus of the paper.

In particular, the has been a substantial amount of work done of the latitude and MLT distributions of electron (and proton) precipitation, particularly at auroral latitudes and at the lower (TED equivalent) energies, such as Cattell et al, 2006, Newell et al, 2009, and more recently, Dombeck et al, 2018 and the references within these. There is also a substantial number of papers on the MLT and latitude dependence and relationship between Alfvén waves and electron precipitation, by the likes of Keiling, Chaston and Hatch. Although these later (Alfvén wave papers) only relate to one small energy band and one part of the precipitation in the channel, so comparison to the presented results would be indirect, so perhaps could not be included in detail. However, the Cattell, Newell and Dombeck papers all show latitude versus MLT plots of precipitation that can and should be compared to the data and results presented in this paper.

Reply: *A couple of comparisons especially with Newell et al. (2009) have been included now. However, the different treatment of energy channels in our paper and in Newell et al. (2009), Dombeck et al. (2018) and Cattell et al. (2006) papers makes a comparison difficult. We are looking at different channels (equivalent to energies) while these authors are looking at number flux and energy flux. Of course number flux and energy flux can be interpreted as low energies and high energies, but a direct one-to-one comparison is not possible. Additionaly, as the reviewer anncounces, it holds only for a very small fraction of our energy spectrum.*

3. Comment

To get precipitation (other than drift lose cone affects in the SAA, which the authors are pointedly not trying to investigate). acceleration and/or wave scattering into the loss cone is necessary. These mechanisms have been discussed and investigated in the literature for decades, and they are dramatically different for the different species and energy channels discussed. All of this has direct relevance to the presented data and the proper and useful interpretation of the results from those data, and the data and results should be discussed from firmly within that context.

Reply: *The following paragraph has been added: "However, it is known that anisotropic distributions occur. While an unaccelerated source population is assumed to be isotropic (as is a wave-scattered fraction of that population in the loss cone) most acceleration processes are connected with an anisotropic pitch angle distribution. Dombeck et al. (2018) lists the most important ones as quasi-static-potential-structures, namely an electric potential field, that may cause isotropic or anisotropic distributions and Alfvén waves, that accelerate only particle energies that are in resonance with magnetic field wave and causes highly anisotropic distributions. Alfvén waves are responsible for electron precipitation during substorms (Newell et al., 2010). According to Newell et al. (2009) electrons are often accelerated while ions are not."*

4. Comment

For the second major issue, the loose use of language, the most egregious issue is the use of the loose use of the word precipitation. In particular, the title and abstract indicates that the paper is about precipitation, but even in the best case this is only half of the presented results, the highest latitude results. As the authors state, the lower latitudes are primarily measuring trapped populations. Therefore the title does not properly describe the paper. Even at the higher latitudes, what is being measured is the downgoing population (centered at various pitch angles depending on latitude, population, and relative potion of the spacecraft to Earth's magnetic pole). While this is still mostly "downward", downward does not necessarily mean precipitating, as the authors point out in relation to their discussion of the SAA. The authors need to be clear what it is that the data presented

are. The title and discussion should be adjusted accordingly.

Reply: *The reviewer is right that we focussed on the precipitation particles at the cost of trapped ones, especially now with erasing the low latitudes section. Our intention was to have the word "precipitation" in the title as it is the main buzz-word for someone who is also doing atmospheric ionization (as we do). Without the low latitude section the title should be more accurate.*
We also agree that the particle flux measured at high latitudes is (without any assumptions) "downgoing" or "downward", while "precipitating" indicates that this flux reaches the top of the atmosphere. In fact considering "downgoing" and "precipitating" as equal -what we did, and which is probably the reviewer's critical point- is possible only when using the assumption of an isotropic pitch angle distribution. If assuming such an isotropical pitch angle distribution the flux decline due to mirroring particles and the flux increase due to a focussing flux tube balance each other (see e.g. Bornebusch et al., 2010) and thus the measured downgoing flux is equal to the precipitating flux. The paragraph now reads: "All figures in this paper are showing differential particle flux in $1/(MeV\,m^2\,s\,sr)$ *as measured, thus we made no assumption about a pitch angle distribution here. However, it should be noted that even if the detector is looking upward (and measuring downgoing particles in high latitudes) it does not necessarily mean that all these particles are precipitating (reaching the atmosphere). Given that some particles are mirroring above the atmosphere a fraction of the downgoing flux is lost, thus the magnetic flux tube is narrowing the particle flux increases again and only in case that the pitch angle distribution is isotrotropic the mirrored fraction is balanced by flux tube narrowing (see e.g. Bornebusch et al., 2010). And only in case of an isotropic pitch angle distribution it does not matter for upscaling which angles of the downgoing pitch angle distribution we are measuring: an isotropic pitch angle distribution may easily be integrated over* 2π *to estimate the total precipitating flux over all angles.*
However, it is known that anisotropic distributions occur. And in that case an estimation of the total precipitating flux is not straight forward as first a pitch angle distribution has to be assumed and second it has to be determined which pitch angles the detector is currently measuring. Since the only other detector orientation on POES is measuring trapped particles (at high latitudes) and since trapped particles do not get lost, there is no reason to assume a smooth transition between these two particle populations. Thus we do not have a "reference" anisotropic pitch angle distribution that might be applied. Applying an isotropic pitch angle (which is often done in literature) will put the downgoing flux on a level with precipitating flux. In case that the paper states "particle precipitation" this isotropic pitch angle distribution has been implicitly assumed. Yet, this has been made without loss of generality since the shown differential flux in that case is equal to the downgoing flux. Thus no transformation is needed."
Additionaly we checked where the "particle precipitation" can be replaced by the more neural word "particle flux".

5. Comment

Additional loose uses of language include discussions of "source" particles, and "qualitative" and "quantitative" results.
In particular, there are really only two sources of particles that are being detected: the solar wind/sun, and the ionosphere/Earth's atmosphere. One could argue that populations that are trapped in the ring current, plasmasphere, radiation belts, plasmasheet, etc, are different pools of particles that are "sources" for the particles measured in study. However, that argument has not been made in the paper. The authors also appear to using the word "source" to allude to both populations pool that the measured particles came from/belong to, and for the mechanisms that cause them to precipitate/be observed in the data. This really needs to be clearly described in the paper.

Reply: *We tried to describe it more clearly now.*

6. Comment

The authors also make a pointed distinction between "quantitative" and "qualitative" results in the paper. In nearly all cases, however, the results described in the paper are qualitative descriptions of the quantitative presented data. The only except to this is the minimum to maximum differences by MLT, which is purely quantitative. Regardless, the use of "qualitative" and "quantitative" as descriptors for the results is unnecessary and as used highly confusing (and inaccurate). As such they should likely just be removed.

Reply: *This section has been completely restructured with breaking up into subsections.*

7. Comment

Several other things that should be addressed in the next version of the paper, include the following: A figure showing coverage by MLT and latitude would be very helpful.

Reply: *This has been added in the new version of Figure 1 as well as in the according description, see also Comment 7. from Reviewer 1.*

8. Comment

A thorough discussion of the minimum count levels of the instruments, and how the noise associated with 1 count levels, interpretation of zero counts, and differences between instruments and channels with regard to this are addressed should be included.

Reply: *The following information has been included: "All shown values are spatial and temporal averaged fluxes. In case that a detector measures zero counts every time it crosses a specific position and at a certain condition this also enters the figures with zero flux (see e.g. Fig. 2, TED electron band 11, isolated substorm, -55 degrees modified APEX latitude at noon). Since the detector counts are transferred into flux the MEPED channels do not recognize flux less than 1 count per integration interval (equivalent to* 1 000 000 $particles/(m^2 ssr)$*, divided by the channels energy range). For the TED detector the tranformation is similar but instead of a fixed number a calibration factor has to be applied for every channel and satellite. The calibrations are given in e.g. Evans und Greer (2004)."*

9. Comment

The field of view of the detectors should be discussed as well as the effects this has in interpretation of the results, from both the perspective of mirroring particles as well as potential anisotropic distributions.

Reply: *We added this paragraph about field of view, particle populations and potential anisotropic distributions.*
"The MEPED detectors have a field of view of ± 15 *degrees, while the TED detector has the following specifications according to Evans und Greer (2006): The field of view of the electron and proton 1000–20 000 eV detector systems are 1.5° by 9°, half angles. The field of view of the 50–1000 eV electron detector system is 6.7° by 3.3°, half angles. The field of view of the 50-1000 eV proton detector system is 6.6° by 8.7°, half angles. Opening angles of the detector in combination with the position of the satellite determines which particle populations the detector is measuring. According to Rodger et al. (2010: Fig. 1) the MEPED 0-degree detector in latitudes discussed in Section 4("High Latitudes") measures particles in the bounce loss cone only. Given that the point of view of the TED detector is almost identical with the MEPED detector and the field of view is significantly smaller, Figure 1 in Rodger et al. (2010) can also be applied, keeping in mind that regions of overlapping particle populations will decline. Thus we can borrow the particle populations seen in the TED channels from the MEPED results. In sum: at high latitudes both detectors count precipitating particle flux while they detect mostly trapped particles at low latitudes.*
All figures in this paper are showing differential particle flux in $1/(MeV\, m^2\, s\, sr)$ *thus we made no assumption about a pitch angle distribution. However, if the pitch angle distribution is isotropic the shown particle flux may easily be integrated over* 2π *to estimate the total precipitating flux over all angles. But it is known that anisotropic distributions occur. In that case an estimation of the total precipitating flux is not straight forward as first a pitch angle distribution has to be assumed and second it has to be determined which pitch angles the detector is currently measuring."*

10. Comment

The word "moves" is used to described the differences between energy channel results. This is not the appropriate word, they are different populations, the features are not "moving" in any sense.

Reply: *Well, if a graph shows a strong increase it is also possible to to describe it with "jumps up" even though it does probably not describe a kangaroo. We tried to avoid "move" and replaced it by "is shifted to", "is displaced to" or "is located at".*

11. Comment

The "precipitation zone" is not at lower latitude with higher energy in general as indicated in the paper. The peak latitude appears identical for TED 8, 11, and 14, for example. The peak "precipitation zone" latitude is related to where particles of these energies reside (radiation belts, etc.) and/or where the acceleration mechanisms that cause those energies occur. This will be clarified once the word is put into appropriate context. It is unclear that there is a physical meaning to the particle energy to latitude of peak flux, so perhaps this relation should be omitted. If it is included, it should be demonstrated with a statistical plot of energy versus peak flux latitude, or some such, from the data.

Reply: *See answer to comment 6. from Reviewer 1.*

12. Comment

The plume has no relevance to the discussion of the 9-10 MLT hotspot, and should not be included in that discussion. This hotspot has been observed before in the Cattell, Newell and Dombeck et al, papers, for example, as well as tangentially addressed in Frey, and should be discussed within the context.

Reply: *The section about low latitudes has been erased.*

Typo

Other details that should be addressed include: Page 1, Line 8: The sentence ending with "how" should be reworded.

Reply: *This sentence as well as approximately every other sentence in abstract, Section 4 and the summary has been reworded.*

Typo

Page 1, Line 13: "main link" should be replaces with something like "a primary link". Solar UV input has much more affect on atmospheric chemistry than particle precipitation, and even affects the precipitation.

Reply: *Replaced by "a primary link" as suggested by the reviewer.*

However we do not agree that UV (generally) has much more affect on atmospheric chemistry than particle precipitation (or why UV radiation should affect the particle precipitation as sugessted by the reviewer).

A nice indication of the impact of particle precipitation in comparison to UV radiation is shown in Wissing et al. (2011: Fig. 6). Here the authors present a comparision of the model chain AIMOS (a model for particle precipitation induced atmospheric ionization) and HAMMONIA (a GCM) with the EISCAT incoherent scatter radar. Electron density during night and day, with and without particle precipitation is calculated and compared to radar measurements. The punch line is that even at day-time the UV component just contributes one fifth of the total electon density (at e.g. 110km altitude). Thus particle precipitation is a (or even the) main driver of atmosperic ion chemistry. Of course this comparison covers the auroral region only, but nobody expects particle precipitation to be a dominant driver of atmospheric chemistry where no particles are precipitating. It would be the same as telling that UV radiation is not dominant during night.

Typo

Page 1, Line 16: The statement the auroral particle precipitation *is due to* ... does not make physical sense. This sentence needs to be reworded.

Reply: *The sentence now reads: Auroral particle precipitation causes production of HO_y and NO_x and thus is a significant player in mesospheric and stratospheric chemistry, especially as these chemicals catalytically impact the ozone cycle (Callis et al., 1996b, a) and subsequently change the radiation budget and affect dynamics.*

Typo

Page 2, Line 22: "over" a wide energy range, rather than "on" a wide energy range.

Reply: *Corrected.*

Typo

Page 6, Line 25: "Of course", rather than "Of cause". Although that is somewhat colloquial, and isn't really required in the sentence.

Reply: *Agreed. The sentence now simply starts with "The SAA ...".*

Typo

Page 8, Line 19: "A potential explanation", rather than "An explanation".

Reply: *Added a few percent of uncertainty with the word "potential".*

References

Asikainen, T. ; Mursula, K. ; Maliniemi, V.: Correction of detector noise and recalibration of NOAA/MEPED energetic proton fluxes. In: *J. Geophys. Res.* 117 (2012), S. A09204. http://dx.doi.org/doi:10.1029/2012JA017593. – DOI doi:10.1029/2012JA017593.

Bornebusch, J.P. ; Wissing, J.M. ; Kallenrode, M.-B.: Solar particle precipitation into the polar atmosphere and their dependence on hemisphere and local time. In: *Advances in Space Research* 45 (2010), Nr. 5, 632 - 637. http://dx.doi.org/https://doi.org/10.1016/j.asr.2009.11.008. – DOI https://doi.org/10.1016/j.asr.2009.11.008. – ISSN 0273–1177.

Callis, L. B. ; Baker, D. N. ; Natarajan, M. ; Bernard, J. B. ; Mewaldt, R. A. ; Selesnick, R. S. ; Cummings, J. R.: A 2-D model simulation of downward transport of NO_y into the stratosphere: Effects on the 1994 austral spring $O_3$and NO_y. In: *Geophys. Res. Lett.* 23 (1996), S. 1905–1908. http://dx.doi.org/10.1029/96GL01788. – DOI 10.1029/96GL01788.

Callis, L. B. ; Boughner, R. E. ; Baker, D. N. ; Mewaldt, R. A. ; Bernard Blake, J. ; Selesnick, R. S.

; Cummings, J. R. ; Natarajan, M. ; Mason, G. M. ; Mazur, J. E.: Precipitating electrons: Evidence for effects on mesospheric odd nitrogen. In: *Geophys. Res. Lett.* 23 (1996), S. 1901–1904. http://dx.doi.org/10.1029/96GL01787. – DOI 10.1029/96GL01787.

Davis, T. N. ; Sugiura, M.: Auroral electrojet activity index AE and its universal time variations. In: *J. Geophys. Res.* 71 (1966), Februar, S. 785–801. http://dx.doi.org/10.1029/JZ071i003p00785. – DOI 10.1029/JZ071i003p00785.

Dombeck, J. ; Cattell, C. ; Prasad, N. ; Meeker, E. ; Hanson, E. ; McFadden, J.: Identification of Auroral Electron Precipitation Mechanism Combinations and Their Relationships to Net Downgoing Energy and Number Flux. In: *Journal of Geophysical Research (Space Physics)* 123 (2018), Dezember, S. 10. http://dx.doi.org/10.1029/2018JA025749. – DOI 10.1029/2018JA025749.

Evans, D. S. ; Greer, M. S.: *Polar Orbiting Environmental Satellite Space Environment Monitor - 2, Instrument Descriptions and Archive Data Documentation.* NOAA Space Environ. Lab, Boulder, Colorado, USA: National Oceanic and Atmospheric Administration, 2004. – 156 S. – Version 1.4b, including TED calibrations.

Evans, D. S. ; Greer, M. S.: *Polar Orbiting Environmental Satellite Space Environment Monitor - 2, Instrument Descriptions and Archive Data Documentation.* NOAA Space Environ. Lab, Boulder, Colorado, USA: National Oceanic and Atmospheric Administration, 2006. – 51 S. – Version 2.0.

Gjerloev, J. ; Hoffman, R. ; Friel, M. ; Frank, L. ; Sigwarth, J.: Substorm behavior of the auroral electrojet indices. In: *Annales Geophysicae* 22 (2004), Juni, S. 2135–2149. http://dx.doi.org/10.5194/angeo-22-2135-2004. – DOI 10.5194/angeo–22–2135–2004.

Green, Janet: NOAA NESDIS-NGDC MEPED Telescope Data Processing ALGORITHM THEORETICAL BASIS / NOAA National Geophysical Data Center. 2013. – Forschungsbericht. – Version 1.0.

Newell, P. T. ; Gjerloev, J. W.: Evaluation of SuperMAG auroral electrojet indices as indicators of substorms and auroral power. In: *Journal of Geophysical Research (Space Physics)* 116 (2011), Dezember, S. A12211. http://dx.doi.org/10.1029/2011JA016779. – DOI 10.1029/2011JA016779.

Newell, P. T. ; Sotirelis, T. ; Wing, S.: Diffuse, monoenergetic, and broadband aurora: The global precipitation budget. In: *Journal of Geophysical Research: Space Physics* 114 (2009), Nr. A9. http://dx.doi.org/10.1029/2009JA014326. – DOI 10.1029/2009JA014326.

Newell, Patrick T. ; Lee, Anna R. ; Liou, Kan ; Ohtani, Shin-I. ; Sotirelis, Thomas ; Wing, Simon: Substorm cycle dependence of various types of aurora. In: *Journal of Geophysical Research: Space Physics* 115 (2010), Nr. A9. http://dx.doi.org/10.1029/2010JA015331. – DOI 10.1029/2010JA015331.

Reeves, G. D. ; Henderson, M. G. ; Skoug, R. M. ; Thomsen, M. F. ; Borovsky, J. E. ; Funsten, H. O. ; C:son Brandt, P. ; Mitchell, D. J. ; Jahn, J.-M. ; Pollock, C. J. ; McComas, D. J. ; Mende, S. B.: IMAGE, POLAR, and Geosynchronous Observations of Substorm and Ring Current Ion Injection. In: Surjalal Sharma, A. (Hrsg.) ; Kamide, Y. (Hrsg.) ; Lakhina, G. S. (Hrsg.): *Disturbances in Geospace: The Storm-substorm Relationship* Bd. 142, 2003 (Washington DC American Geophysical Union Geophysical Monograph Series), S. 91.

Rodger, Craig J. ; Clilverd, Mark A. ; Green, Janet C. ; Lam, Mai M.: Use of POES SEM-2 observations to examine radiation belt dynamics and energetic electron precipitation into the atmosphere. In: *Journal of Geophysical Research: Space Physics* 115 (2010), Nr. A4. http://dx.doi.org/10.1029/2008JA014023. – DOI 10.1029/2008JA014023.

Wissing, J. M. ; Kallenrode, M.-B. ; Kieser, J. ; Schmidt, H. ; Rietveld, M. T. ; Strmme, A. ; Erickson, P. J.: Atmospheric Ionization Module Osnabrck (AIMOS): 3. Comparison of electron density simulations by AIMOS-HAMMONIA and incoherent scatter radar measurements. In: *Journal of Geophysical Research: Space Physics* 116 (2011), Nr. A8. http://dx.doi.org/10.1029/2010JA016300. – DOI 10.1029/2010JA016300.

Magnetic local time asymmetries in precipitating electron and proton ~~precipitation~~ populations with and without substorm activity

Olesya Yakovchuk[1,2] and Jan Maik Wissing [1]

[1]The Institute of Environmental Systems Research, University of Osnabrück, Osnabrück, 49069, Germany
[2]Skobeltsyn Institute of Nuclear Physics, Lomonosov Moscow State University, Moscow 119234, Russia

Correspondence: Olesya Yakovchuk (oyakovchuk@uos.de)

Abstract. The magnetic local time (MLT) dependence of electron (0.15–300 keV) and proton (0.15–6900 keV) precipitation into the atmosphere based on National Oceanic and Atmospheric Administration POES and METOP satellites data during 2001–2008 was described. Using modified APEX coordinates the influence of particle energy, substorm activity and geomagnetic disturbance on the MLT flux distribution was statistically analysed.

Some of the findings are: a) ~~MLT flux differences of up to 1:2[5] have been localized inside the auroral oval~~Substorms mostly increase particle precipitation in the night-sector by about factor 2–4 but can also reduce it in the day-sector. b) MLT dependence can be assigned to ~~different particle sources and~~ particles entering the magnetosphere at the cusp region and magnetospheric particles in combination with energy-specific drifts. c) MLT flux differences of up to two orders of magnitude have been identified inside the auroral oval during geomagnetically disturbed conditions. d) The maximum flux asymmetry ratio depends on particle energy, ~~but not necessarily on geomagnetic disturbance. For protons it is invariant with Kp , for electrons the dependence varies with Kp and kinetic energy defines how. c) Substorms mostly increase particle precipitation in the night-sector by about factor 2–4 but can also reduce it in the day-sector~~decreasing with Kp for low energetic particles and increasing with Kp for higher energy electrons, while high energy protons show a more complex dependency.

~~Finally we have a look at MLT-dependent trapped particle flux in the plasmasphere, which shows vast and abstract MLT differences.~~

1 Introduction

Particle precipitation is ~~the main~~ a primary link between solar activity and atmospheric chemistry. Thorne (1977) suggested a depletion of Ozone in 40–80 km through production of nitric oxides by precipitation of relativistic radiation belt electrons. Ozone depletion following solar energetic particle events (mostly protons) has been observed in the same year (Heath et al., 1977). Auroral particle precipitation ~~is due to production and downwelling~~ causes production of HO_y and NO_x and thus is a significant player in mesospheric and stratospheric chemistry, especially as ~~it catalytically impacts~~ these chemicals catalytically impact the ozone cycle (Callis et al., 1996b, a) and subsequently ~~changes~~ change the radiation budget and ~~affects~~ affect dynamics. Consequently there has been an immanent need for the description (and later on modelling) of the particle precipitation. And even though the investigation of precipitation pattern of low energetic particles (and especially electrons) started more then

30 years ago (Hardy et al., 1985, e.g.), the rising vertical extend of climate models has shifted the focus from high energetic particles to lower energies again.

The interplanetary medium is the driver of geomagnetic disturbance and may compress, deform or reconnect to the magnetosphere. Meredith et al. (2011) e.g. states that on average, the flux of precipitating energy electrons (E>30 keV) is enhanced by a factor of about 10 during the passage of the high-speed stream (geomagnetic storm time) at all geographic longitudes. Thus geomagnetic disturbance should be considered in a description of particle precipitation.

~~Magnetic local time~~ MLT dependence is a result of charge-dependent drift directions (Allison et al., 2017) and (linked to that) opposite potentials in field-aligned Birkeland-currents. The authors themselves note that the particle flux variety in different local time sectors may reach an order of magnitude, with proton precipitation dominating in evening and night sectors and electrons dominating in morning and night (Wissing et al., 2008).

Substorms are either directly driven or/and loading processes, where energy is accumulated and released abruptly in the Earth's magnetosphere (Akasofu, 2015). The global morphology of auroral substorms has first been described by Akasofu (1964) using simultaneous all-sky camera recordings from Siberia, Alaska and Canada. Later space-born missions like e.g. the UV photometer mission on Dynamics Explorer 1 (DE-1) (Frank et al., 1981) confirmed this morphology.

Akasofu et al. (1965) also already characterized the expansion phase and the recovery phase of a substorm (a preceding growth phase has been added by McPherron (1970)). Due to auroral emissions the substorms were associated with excitation and ionization by precipitating particles that have been investigated by ground based riometers (Berkey et al., 1974) and later on by satellite missions (e.g. Fujii et al., 1994), observing intense energetic electron precipitation in or near the onset/surge region. The energy range of the precipitating particles has been defined as electrons and protons at approx. 10–100keV with a low-energy cut-off (Birn et al., 1997). The precipitation regions depend on particle species.

The occurrence of substorms depends on the orientation of the interplanetary magnetic field (Reeves et al., 2003). As shown in Reeves et al. (2003) these external solar wind parameters subsequently impact the magnetic field on the ground and are represented in the ~~AE index. In this study we use the SML index to define substorm onsets, which is the lower envelope of the SME,~~ Auroral Electrojet (AE) index. Auroral Electrojet indices AE=AU-AL are a good proxy of the global auroral power, where AU and AL are the upper and lower components of AE, which means the largest and smallest values of the H component among 12 magnetic stations (Davis and Sugiura, 1966). AU represents the strength of the eastward electrojet, while AL represents the westward electrojet. Consequently AL seems to be the index which best corresponds to westward intensification of the auroral current aka substorm activity. Prior to substorm onset, AL index is typically small in magnitude, with the contributing station near dawn, whereas during substorm onset, the station contributing to the lower envelope is usually in the dusk sector under the auroral expansion. However, due to the limited spatial coverage of the 12 magnetometer stations the auroral expansion can be missed, which means that this index does not always reflect the onset (Gjerloev et al., 2004). The use of SuperMAG SML, an index derived likewise to the AE but based on all available magnetometer stations ~~in these latitudes(Newell and Gjerloev, 2011a).~~ (typically more than 100) at these latitudes, considerably improves the detection of substorm onsets (Newell and Gjerloev, 2011a). Thus we use the SML index in this study to define substorm onsets.

In this study we will discuss MLT differences in particle ~~precipitation on~~ fluxes (and precipitation) over a wide energy range and show how substorms impact this pattern.

In Section 2 particle data, modified APEX coordinate system, SML and Kp-binning will be introduced. Section 3 displays the application of modified APEX coordiantes to the ~~precipitation maps~~flux maps, discusses special aspects of the MLT binning and illustrates how the auroral oval is fitted. In Section 4 ~~and ?? we will analyse the particle precipitation~~ the main discussion follows, the analysis of particle fluxes on high latitudes~~and low latitudes, respectively~~. The results are summarized in Section 5.

2 Data sets

This section describes the data sets and how the data has been processed.

2.1 Particle data

For particle ~~precipitation~~ data we use time series (2001–2008) of 16 s averaged electron fluxes ranging from 0.15 to 300 keV and protons from 0.15 to 6900 keV measured on board the polar orbiting NOAA/POES and their successor, the ~~MetOp~~ METOP satellites (Evans and Greer, 2006). 2001 to 2008 covers the complete declining phase of solar cycle 23 and thus includes very active (sometimes extreme) to very low activity periods ~~. Information about the different channels can be found in Tab. 1.~~ (Logachev et al., 2016).

In total all available data from POES 15, 16, 17, 18 and ~~MetOp~~ METOP 02 has been used, except for POES 16 after 2006 as it is known that the TED data is erroneous.

~~Channels from the POES and METOP satellites which have been used.~~

All satellites have sun-synchronous orbits at altitudes around 820 km (with ≈ 100 minute periods of revolution) and an inclination of $\approx 98.5°$. The satellites have initially been placed in orbits that cross the equator in a fixed local time either being morning-evening or day-night sector. However, or in our case ~~furtunately~~fortunately, these orbits were drifting slightly with time. Thus our long sample period and the moving five satellites allowed us to investigate the effect of local time on particle ~~precipitation~~fluxes.

~~It should be said that the particle detectors suffer from various contamination effects:~~

~~The MEPED electron channels are highly efficient detectors for high energetic protons.In order to avoid contaminated electron data we excluded MEPED electrons when the omnidirectional proton channel P7 showed more than 2 counts (based on high resolution 2 s data). This does not only cut out probably contaminated periods in SPEs, but also the region of the SAA. The MEPED electron channels have been substracted from each other, resulting in differential channels~~Information about the different channels can be found in Tab. 1. All particle count rates have been converted into differential flux by dividing the energy range and a geometric factor has been applied as suggested in Evans and Greer (2006).

It is known that there is no adequate upper energy threshold of the three MEPED electron channels (Yando et al., 2011). In order to work with specific energy bands we subtracted sequent channels, resulting in the two channels mep0e1-e2 and mep0e2-e3 with the energy bounds given in Tab. 1.

Table 1. Channels and nominal energy ranges from the POES and METOP satellites which have been used.

	instrument	channel	energy range
electrons	TED	band 4	154–224 eV
		band 8	688–1000 eV
		band 11	2.115–3.075 keV
		band 14	6.503–9.457 keV
	MEPED	mep0e1-e2	30–100 keV
		mep0e2-e3	100–300 keV
protons	TED	band 4	154–224 eV
		band 8	688–1000 eV
		band 11	2.115–3.075 keV
		band 14	6.503–9.457 keV
	MEPED	mep0P1	30–80 keV
		mep0P2	80–240 keV
		mep0P3	240–800 keV
		mep0P4	0.8–2.5 MeV
		mep0P5	2.5–6.9 MeV

~~It should be mentioned that we~~

We used the 0° detectors only. While the TED 0°-detector looks exactly radially outward the MEPED 0°-detector is slightly shifted by 9° to ensure a clear field of view (Evans and Greer, 2006). ~~In~~

The MEPED detectors have a field of view of ± 15 degrees, while the TED detector has the following specifications according to Evans and Greer (2006): The field of view of the electron and proton 1000–20 000 eV detector systems are 1.5° by 9°, half angles. The field of view of the 50–1000 eV electron detector system is 6.7° by 3.3°, half angles. The field of view of the 50–1000 eV proton detector system is 6.6° by 8.7°, half angles. Opening angles of the detector in combination with the position of the satellite determines which particle populations the detector is measuring. According to Rodger et al. (2010, Fig. 1) the MEPED 0-degree detector in latitudes discussed in Section 4 measures particles in the bounce loss cone only.

Given that the point of view of the TED detector is almost identical with the MEPED detector and the field of view is significantly smaller, Figure 1 in Rodger et al. (2010) can also be applied, keeping in mind that regions of overlapping particle populations will decline. Thus we can borrow the particle populations seen in the TED channels from the MEPED results. In sum: at high latitudes both detectors count precipitating particle flux while they detect ~~trapped particles in~~ mostly trapped particles at low latitudes.

All figures in this paper are showing differential particle flux in $1/(MeV\,m^2\,s\,sr)$ as measured, thus we made no assumption about a pitch angle distribution here. However, it should be noted that even if the detector is looking upward (and measuring downgoing particles in high latitudes) it does not necessarily mean that all these particles are precipitating (reaching the atmosphere). Given that some particles are mirroring above the atmosphere a fraction of the downgoing flux is lost, thus the magnetic flux tube is narrowing the particle flux increases again and only in case that the pitch angle distribution is isotrotropic the mirrored fraction is balanced by flux tube narrowing (see e.g. Bornebusch et al., 2010). And only in case of an isotropic pitch angle distribution it does not matter for upscaling which angles of the downgoing pitch angle distribution we are measuring: an isotropic pitch angle distribution may easily be integrated over 2π to estimate the total precipitating flux over all angles.

However, it is known that anisotropic distributions occur. While an unaccelerated source population is assumed to be isotropic (as is a wave-scattered fraction of that population in the loss cone) most acceleration processes are connected with an anisotropic pitch angle distribution. Dombeck et al. (2018) lists the most important ones as quasi-static-potential-structures, namely an electric potential field, that may cause isotropic or anisotropic distributions and Alfvén waves, that accelerate only particle energies that are in resonance with magnetic field wave and causes highly anisotropic distributions. Alfvén waves are responsible for electron precipitation during substorms (Newell et al., 2010). According to Newell et al. (2009) electrons are often accelerated while ions are not.

In case of an anisotropic pitch angle distribution an estimation of the total precipitating flux is not straight forward as first a pitch angle distribution has to be assumed and second it has to be determined which pitch angles the detector is currently measuring. Since the only other detector orientation on POES is measuring trapped particles (at high latitudes) and since trapped particles do not get lost, there is no reason to assume a smooth transition between these two particle populations. Thus we do not have a "reference" anisotropic pitch angle distribution that might be applied. Applying an isotropic pitch angle (which is often done in literature) will put the downgoing flux on a level with precipitating flux. In case that the paper states "particle precipitation" this isotropic pitch angle distribution has been implicitly assumed. Yet, this has been made without loss of generality since the shown differential flux in that case is equal to the downgoing flux. Thus no transformation is needed.

All shown values are spatial and temporal averaged fluxes. In case that a detector measures zero counts every time it crosses a specific position and at a certain condition this also enters the figures with zero flux (see e.g. Fig. 2, TED electron band 11, isolated substorm, -55 degrees modified APEX latitude at noon). Since the detector counts are transferred into flux the MEPED channels do not recognize flux less than 1 count per integration interval (equivalent to 1 000 000 particles/$(m^2 ssr)$, divided by the channels energy range). For the TED detector the tranformation is similar but instead of a fixed number a calibration factor has to be applied for every channel and satellite. The calibrations are given in e.g. Evans and Greer (2004).

The particle detectors suffer from various contamination effects: The MEPED electron channels are highly efficient detectors for high energetic protons. In order to avoid contaminated electron data we excluded MEPED electrons when the omnidirectional proton channel P7 showed more than 2 counts (based on high resolution 2 s data). This does not only cut out probably contaminated periods in SPEs, but also the region of the SAA. The MEPED electron channels have been substracted from each other, resulting in differential channels.

Note that the given energy ranges taken from Evans and Greer (2006) are nominal. Some channels suffer from degradation. This mostly holds for the MEPED proton channels and is a result of structural defects caused by the impinging particles. On the long run it causes an energy shift (to higher particles energies) since less electron-hole pairs are produced per deposited particle energy. Consequently the energy ranges mentioned are nominal ranges. Further details on degradation of the MEPED channels can be found in e.g. Asikainen et al. (2012).

2.2 Coordinate system

A meaningful representation of particle precipitation has high requirements for the coordinate system as they are: a) The ~~precipitation~~ flux pattern should be invariant in time even though the magnetic field is changing (meaning moving poles, not magnetospheric distortion). This is needed for the long investigation period as well as for durability of forecasts. b) The latitude of particle ~~precipitation~~ flux pattern should be invariant of the longitude. Given this criterion the longitude may be replaced by local time as second coordinate. c) If the previous criterion is applied, it includes that particle flux has to be recalculated. Following the footpoints of two shells with a distinct magnetic field strength, their latitudinal distance differs with longitude. Since the particle flux is measured on a fixed detector size this has to be taken into account when removing the longitudinal dependence. d) Particle measurements take place at the position of the satellite, which is in about 820 km above the ground. But the effect of particle precipitation (the atmospheric ionization) is mainly located ~~in~~ at about 110 km altitude (maximum of magnetospheric ionization, higher particle energies cause ionization futher down). Consequently a coordinate system that allocates the satellite's measurement to their respective position at 110 km altitude would be helpful.

The coordinate system that allows for all named requirements is the modified APEX coordinate system (Richmond, 1995). The coordinates are variable in time using the International Geomagnetic Reference Field model magnetic field configuration, which means they also reflect the temporal movement of the poles. Richmond (1995) present three coordinate systems which are closely connected. The quasi-dipole (QD) coordinates present the magnetic latitude and longitude on the ground (Richmond, 1995, see f1 and f2 base vectors in Fig. 1), while the third base vector goes radially outward. The APEX coordinate system is using the same longitude, but the latitude is following the magnetic field lines as propagating (precipitating) particles

do, meaning that a charged particle is always on the same latitude. The APEX latitude is defined by its footpoint on the QD latitude on the surface. In the *modified* APEX coordinates not the surface but an arbitary altitude is used for the definition of the latitude, e.g. that altitude where particles cause the ionization, in our case 110 km above the ground. Thus the measurements should be mapped down on the according field line until it reaches the altitude where the particle is stopped by the atmosphere (about 110 km). In all (modified) APEX systems measurements and ionization location are on the same latitude. Thus a desirable coordinate system for our work is the modified APEX system.

2.3 SML index and derived substorm onsets

The period 2001–2008 was chosen for our investigation, where all necessary data about substorms and particle ~~precipitation~~ fluxes are available. For the identification of substorm events, we use the technique published by Newell and Gjerloev (2011a). The substorm onset is determined by the auroral electrojet SML index, which is derived from magnetometer data obtained by the SuperMAG magnetometer network. The SuperMAG magnetometer network in the northern hemisphere (up to 100 stations) improves the traditional auroral electrojet (AL) network (12 stations) (Newell and Gjerloev, 2011a).

Newell and Gjerloev (2011b) distinguish recurrent and isolated substorms. While recurrent substorms appear in groups with less than 82 min between their onsets, the isolated substorm onsets are separated by at least 3 h. Only the isolated substorms are used in our investigation, as this helps to ~~avoide~~ avoid two or more substorms overlapping each other. Contrasting the isolated substorm periods we also use time periods without any substorms (no-substorm period). The total number of substorm onsets for our period constitutes 15 316 events. Defining 30 min after an onset as typical length of a substorm, we end up with 10.4% of the whole period being generally substorm-influenced (while the rest is no-substorm). However, just 1.87% of the whole period can be attributed to isolated substorms.

It should be noted that with this technique we are not able to separate different substorm phases nor can we distinguish different types of substorms. ~~Independend~~ Independent from substorm phase, the proton aurora is displaced equatorward of the electron aurora for dusk local times, and it is poleward for dawn local times. In the onset region however, proton and electron precipitation depends on the substorm phase and may even be colocated (Mende et al., 2003). Thus the results represent a mean substorm value.

2.3.1 Kp-binning of particle data

The Kp-index is a three-hourly index estimating the geomagnetic activity (Bartels et al., 1939). In contrast to the AL/SML index which describes the auroral electrojet activity, the Kp-index is sensitive to several current systems (e.g. the ring current) and thus describes the magnetospheric activity with a more global perspective.

The particle data has been binned into ~~three~~ 11 partly overlapping Kp-level groups~~. These levels have been chosen in a way that each bin contains approx. the same amount of 3-hour periods: Kp~~ : 0–0.7, 0–1~~(quiet): 7660, Kp~~ , 1–1.7, 1.3~~–2.3 (less quiet): 7666 and Kp 2.7-9 (unsettled to storm): 8050. This sums up to the 8 year period.However, as~~ –2.3, 2–2.7, 3–3.7, 4–4.7, 5–5.7, 6–6.7, 6–9 and 7–9. As the Kp-levels are not equally populated (low Kp-levels occur more frequently than e.g. 6–6.7), the amount of satellites is not constant, the substorms are not evenly distributed in time and the local time sectors are not

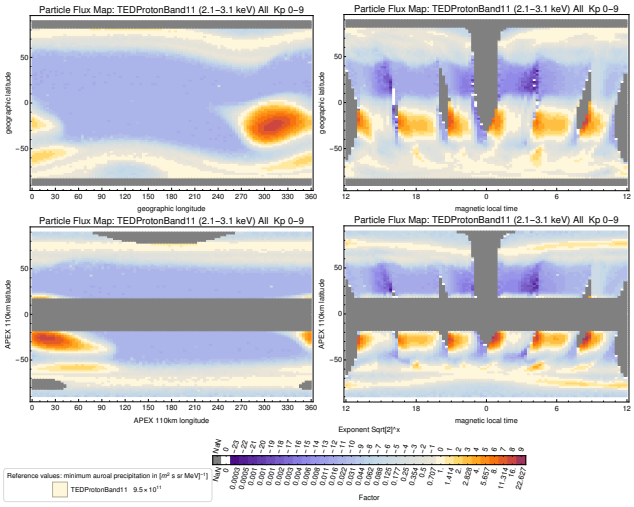

Figure 1. Particle flux in the TED proton band 11 in geographic and modified APEX 110 km coordinates. The color scale marks the minimum flux in the auroral oval in beige. The neighbouring color indicates that the flux is a factor $\sqrt{2}$ apart (the neighbour after that a factor 2).

evenly covered, single data points (with 1 h MLT-resolution, 2 degrees latitudinal resolution and the Kp-binning) may contain a different amount of the 16 s averages.

3 ~~Precipitation~~ Particle flux map

Binning of particle flux strongly depends on the coordinate system. Some features are determined by the inner magnetic field and thus co-rotating with Earth, while others are influenced by the interaction with the solar wind and according to that fixed in relation to the Sun and to the (magnetic) local time. Since we will use the modified APEX coordinates in this paper we will have a look how the particle flux representation differs to geographic coordinates and which aspects can be best described in the two systems.

Figure 1 shows the TED proton band 11 in geographic coordinates (top row) and modified APEX 110 km coordinates ~~.~~ (bottom row). The left column shows latitude against longitude while the right column shows latitude against MLT. No selection according to Kp-level or substorm intensity has been made, while all available data from ~~MetOP~~ METOP 2 and POES 15, 16, 17 and 18 for the years 2001–2008 has been included. This allows a spatial resolution of 3.75 degrees longitude (or 15 min MLT). Please note that latter figures show a reduced longitudinal resolution of 15 degrees (or 1 h MLT) only to avoid statistical noise in e.g isolated substorms periods.

Most obvious in the geographic representation (Fig 1, top, left) is the South Atlantic Anomaly (SAA, located roughly between ~~-70 and 0~~ 280 and 360 degrees East and -45 to 0 degrees North). Being a dip in the geomagnetic field, the SAA allows energetic particles in the radiation belt to reach altitudes low enough to be reached by the satellite's orbit. According to Rodger et al. (2010, Fig. 1) the particle population in the SAA consists of particles precipitating in bounce and drift loss cone

as well as trapped particles. Thus the high flux values are not necessarily connected to high particle precipitation. As the SAA is a geomagnetic feature it is co-rotating and thus best represented in the geographic coordinates, while a MLT based coordinate system intermixes SAA patterns with non SAA patterns on the same latitude. However, in contrast to our expectations the SAA in MLT representation is not evenly smeared out over all latitudes. A detailed discussion on this follows in Section 3.1.

A feature that is connected to the SAA is the particle precipitation ~~in~~ of the drift loss cone. Particles drift around Earth and bounce between the mirror points. These mirror points get to lowest altitudes where the magnetic field is weakest. Since the geomagnetic field around the SAA is weak the dominating particle precipitation zone is where these field lines have their foot points. In Fig. 1 (~~upper panel~~top, left) this can be clearly identified South-East of the SAA. In the northern hemisphere the particle precipitation due to the drift loss cone is less dominant, but still visible.

Figure 1 (top, right) shows the same data on a geographic latitude vs. MLT grid. As the auroral oval is not visible as an oval any more but mixes up local time differences and the latitudinal variations that can already be seen in Fig. 1 (top, left).

Apart from that the geographic representation is not very helpful. Due to the satellites' inclination the poles are not covered and typical pattern as the auroral precipitation is meandering.

Switching to magnetic ~~coordinates (here:~~ modified APEX 110 km coordinates (see Fig 1, bottom, left) straightens the auroral oval and mostly removes the longitudinal dependence ~~(not shown)~~except for the SAA and the drift loss cone in the South of the SAA. Consequently we can replace the APEX longitude by MLT (see Fig. 1, ~~lower panel). Of cause the~~ bottom, right). Features that depend on MLT now become visible and the auroral oval itself does not show a hemispheric dependence. The SAA and the drift loss cone, however, are now smeared out ~~(see e.g. double auroral structure)~~ and still produce a hemispheric asymmetry~~, but features that depend on the local time now become visible and the auroral oval itself does not show a hemispheric dependence.~~ . The drift loss cone that is located at a distinct modified APEX 110 km longitudinal range even appears as an double auroral structure at the same latitude but covering all longitudes. Which of course is an artifact of this kind of MLT binning.

Most obvious in the modified APEX/MLT coordinates (see Fig. 1, bottom, right) are the local time dependencies in the auroral zone as well as ~~in~~ at lower latitudes. Substorm ~~depended~~ dependent precipitation that mostly appears during night time can also be identified (see following sections).

Some regions in modified APEX/MLT coordinates will never be reached as the local time coverage is limited. This holds for the midnight hours in the northern hemisphere as well as for noon ~~in low latitudinal Southern~~ at low latitudinal southern hemisphere. The equatorial region seems not to be covered, however, is not a data gap. The flux is mapped to the latitude where the guiding field-line hits 110 km. Since the satellites cross the (dip) equator at 850 km all field lines peak below that point are not covered (<19 degrees N/S). Since the magnetic poles are shifted to the geographic ones the satellites' inclination does not limit the polar coverage.

As a consequence of the regional coverage and SAA influence we will select the Southern hemisphere auroral zone ~~and the low latitudes in Northern hemisphere~~for further investigation.

3.1 Why is the SAA not evenly smeared out over all longitudes?

If we would take a look at the footpoints of a solar-synchronous satellite in local time we would see that it always crosses a particular latitude e.g. the equator at one particular local time in ascending mode (and another, at the equator 12 hours later, in descending mode). At high latitudes it crosses 12 local time zones on a few latitudes, but still, the next orbit will exactly match the first (except if the orbit moves, which also happens to the POES/METOP satellites, but on longer time scales). Looking at the footpoints of the same satellite in MLT changes quite a bit. Given that the MLT zones are based on magnetic latitude and the magnetic poles being shifted, it means that the MLT-footpoints especially in high latitudes differ significantly from one orbit to the next. Due to the POES inclination of 98.5 degrees the satellite may at maximum reach the northern magnetic pole. The southern magnetic pole however, may not only be reached but even passed.

Thus there are two options how the MLT during an orbit may develop in the southern hemisphere: If the satellite's longitude is far from the magnetic pole the orbit will not pass the magnetic pole and the MLT will gradually increase by 12 hours till it reaches the equator in ascending mode again. Let us call this "ascending MLT". In the other case ("descending MLT"), the southern magnetic pole will be passed and the MLT zones will be flown through in the opposite direction, decreasing MLT by 12 hours till reaching the equator in ascending mode again. Since the southern magnetic pole is somewhat south of Australia a significant fraction of the orbits passing it will cross the SAA in descending mode (but not in ascending mode). The opposite is true for the ascending MLT path, which includes a significant fraction of orbits that pass the SAA in ascending mode.

In case multiple satellite are used this does not affect high latitudes, but in low latitudes the situation is different. Since the satellites are crossing the equator at two specific local times (for ascending and descending mode, being just slightly broader in MLT), MLT coverage at the equator is limited to these points. They however may be reached in ascending mode (or left in descending mode) by ascending or descending MLT paths. In Fig. 1, top right (or bottom right) the equator is crossed at six different smeared out MLTs. While the ones on the left (13, 17 -two satellites- and 21 MLT) represent the descending mode, the ones on the right (1, 5 and 9 MLT) are in ascending mode.

The ascending MLT path now connects e.g. the low flux right edge of the 21 MLT equatorial crossing with the high flux (SAA) left edge of the 9 MLT equatorial crossing. The descending MLT path on the other side connects e.g. the high flux (SAA) left edge of the 21 MLT equatorial crossing with the low flux right edge of the 9 MLT equatorial crossing.

In sum the ascending and descending MLT paths cause the left edge of an equatorial crossing to be affected by the SAA, while the right edge is not. Any MLT analysis of low latitudes based on POES/MEPED will suffer from the fact that the longitudes contribute very unevenly to the MLT zones. This hampers a flux analysis in low latitudes. In high latitudes however this effects gets counterbalanced by broader MLT coverage and multiple satellites.

3.2 Determination of the auroral oval

In some parts of the paper we will refer to APEX 110 km latitude or MLT locations of the auroral oval or its flux maximum and minimum. These locations have been determined automatically. A routine determines the maximum flux for each MLT-bin within the typical auroral latitude range. This results in a preliminary auroral oval. Then the latitudinal differences between MLT-predecessor and successor are determined and in case of large outliers a point is assumed to be a spike in the data and replaced by the next biggest flux-bin in that MLT zone. In case that more than 7 points have to be replaced for a auroral oval

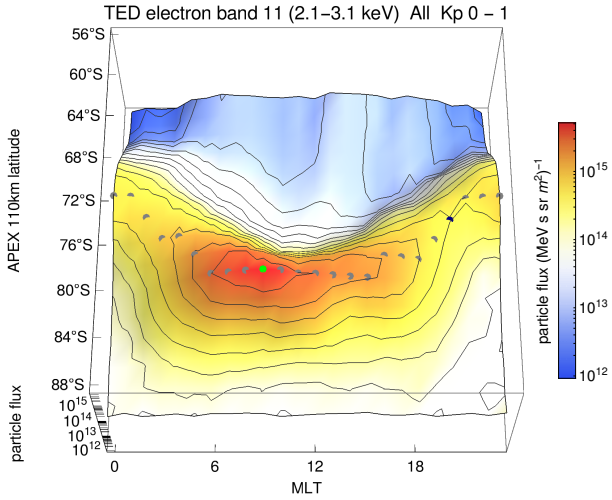

Figure 2. Sample for an auroral oval fit. The gray dots represent the position of the auroral oval. The green (9 MLT) and black (20 MLT) dots indicate maximum and minimum of the auroral oval, respectively.

the according channel-Kp set is neglected. In sum this ends up in a well-working detection algorithm for the auroral oval and allows us to find its minimum and maximum flux, or their ratio. A sample is given in Figure 2. All locations have been cross-checked manually.

4 ~~High Latitudes~~Particle flux at high latitudes

Figure 3 shows the precipitating electron flux ~~in~~ at high latitudes in the southern hemisphere. The southern hemisphere has been chosen to ~~avoide~~ avoid the data gaps between 23 and 1 MLT in the northern hemisphere (see the ~~Section ??~~Fig. 1, bottom right). Apart from that, northern and southern hemisphere do not show significant differences in APEX coordinates.

The color scale is logarithmic with a base of two, meaning the threshold to the adjacent color is a factor of 2 apart. The reference value has been set individually for every channel to the lowest occurring value inside the auroral oval. Thus local time differences can be easily identified and quantified. No-substorm periods (left panel) and isolated substorm periods (right panel) for all electron channels are given here.

Figure 4 shows the same as Figure 3 but for protons.

~~Comparing these~~

Comparing the two panels of Fig. 3 and 4, we can identify:

1. ~~Generally, the main **precipitation zone** (white to reddish colours)**moves equatorward with increasing particle energy**.~~

Typical pattern in low energetic channels (see Section 4.1),

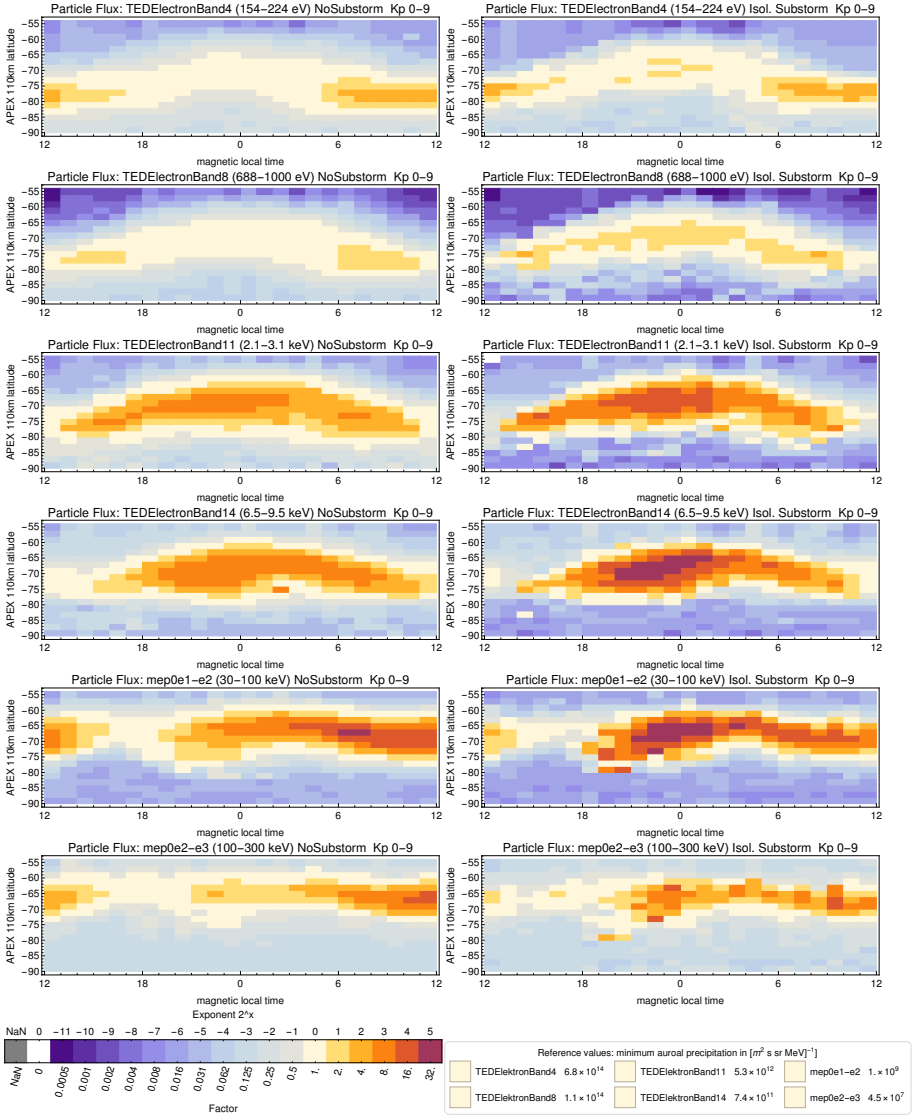

Figure 3. Electron flux in various channels ~~in~~ at high latitudes on the southern hemisphere. Left panel shows periods without substorms, right panel gives periods with isolated substorms only.

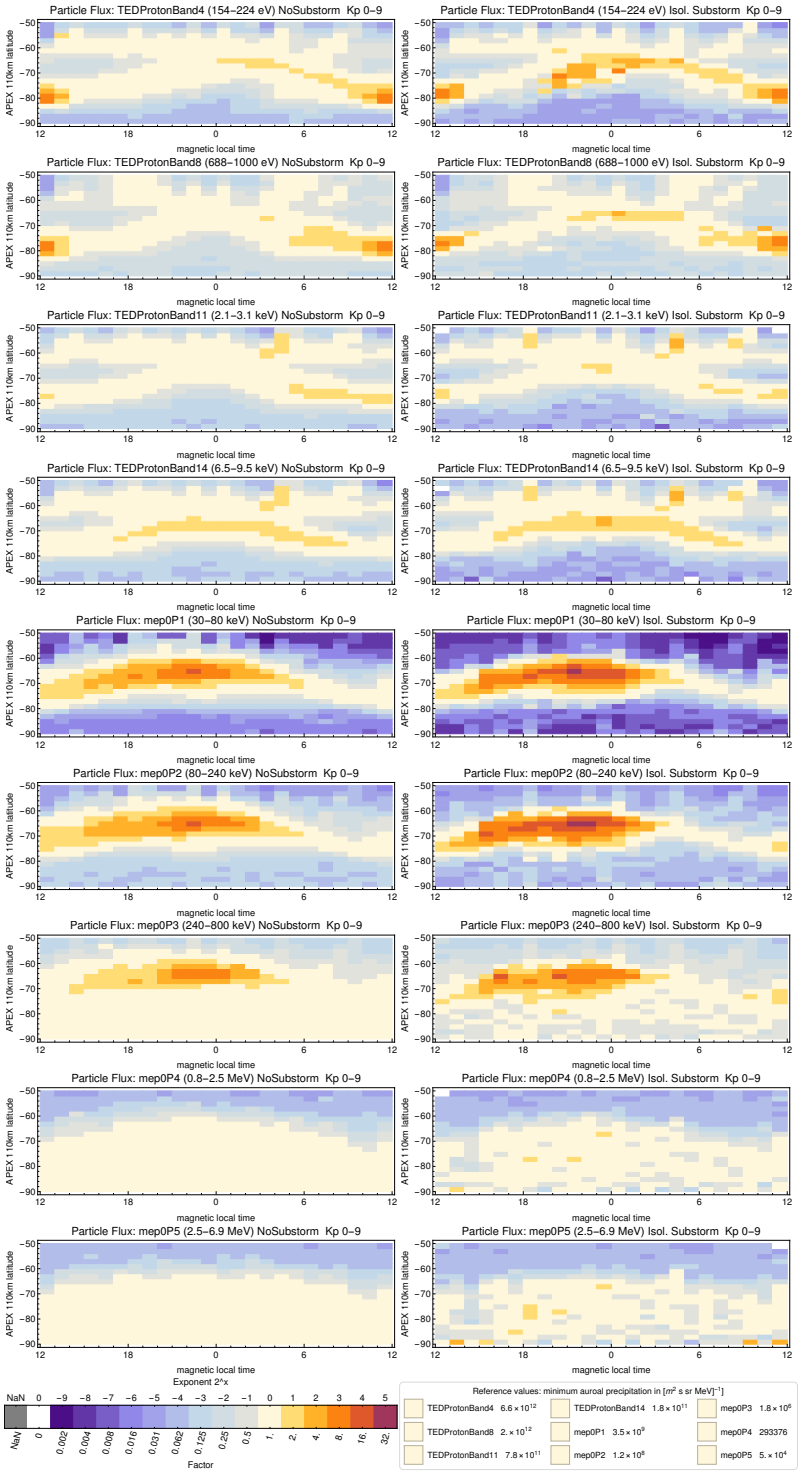

Figure 4. Proton flux in various channels at high latitudes on the southern hemisphere.

2. ~~Quantitatively, the particle precipitation shows distinct MLT dependence. The range of this dependence changes with particle energy. While the two **lowest TED electron channels (band 4 and 8) show just minor MLT variations, in the higher particle energies it varies by more than one order of magnitude**.~~

   ~~**During** isolated **substorms** the maximum local time **differences are similar or a factor of 2 higher** (and the maximum is located in the midnight sector during substorms , see next paragraph). For details and a summary of other (not shown) Kp-bins, see Table **??**.~~

   Typical pattern in high energetic channels (see Section 4.2),

3. ~~Qualitatively, MLT variations also depend on particle energy:~~ Kp-dependence of the auroral MLT-asymmetry (see Section 4.3),

4. ~~The **higher particle channels** (above >2 keV) **show a movement of the main precipitation with MLT from midnight** (~~Auroral oval asymmetry during substorms (see Section 4.4), and a

5. Latitudinal displacement of the maximum auroral flux depending on Kp and energy (see Section 4.1).

4.1 Typical pattern in low energetic channels

Low energetic proton and electron channels, namely TED electron band ~~11) **via morning sector** (mep0e1-e2corr) **to day sector** (mep0e2-e3corr). An explanation for the movement in the higher electron channels(and the opposite directed movement of the protons) is the westward partial ring current in the night side which is closed by flied-aligned currents (Birkeland Region 2) into the ionosphere (Lockwood, 2013; Milan et al., 2017). While electrons in ring current drift eastwards and thus may precipitate predominantly in the morning sector, the protons undergo a westward drift and mainly precipitate in the evening sector. The energy dependence might be due to different drift velocities (Allison et al., 2017). A drift of electron precipitation (>20 keV) towards the dayside has also been reported by Matthews et al. (1988); Newell and Meng (1992); Østgaard et al. (1999) and is associated with central plasmasheet electron injections in the midnight region. The resulting dawn-dusk asymmetry for electrons also depends on Kp-level.~~

~~The maximum **MLT-asymmetry depends on Kp: for the low energetic channels** band~~ 4 and 8 ~~**it decreases** with Kp, in band~~ as well as proton band 4, 8 and 11 ~~it stays the same but **for**~~ show a very different spatial pattern than the higher channels.

The maximum flux in the ~~**more energetic**~~ auroral oval appears in the day sector. TED electron band ~~14, mep0e1-e2 and mep0e2-e3 (where it shows a clear dawn-dusk asymmetry) **it increases with Kp**. In the Kp-bins chosen for our study it doubles from bin to bin (see Table **??**). And even for Kp 0–1 the dawn-dusk asymmetry stays visible with a factor of about 2 to~~ 4 ~~in TED electron band 14~~ and ~~mep0e1-e2 (not shown but same pattern as in Fig. 3).~~ 8 peak between 6 and 17 MLT. This agrees e.g. very well with the monoenergetic electron number flux for low solar wind driving (Fig. 7 in Newell et al., 2009).

~~**For** isolated **substorms the movement is** the same, but **superimposed with** substorm-specific **night-side** (20–2 MLT) **particle precipitation** which reflects the substorm electrojet manifestations (Lockwood, 2013; Milan et al., 2017). The electron~~

precipitation intensity at midnight sector outnumbers the no-substorm values at the same place by factor 2 to 4. For mep0P1 to mep0P3 the evening sector is slightly increased during substorms.

The **lower TED electron band 4 and 8 peak between 6 and 17 MLT**. The proton bands are even more concentrated around noon but show an additional slight increase from noon via the morning sector towards midnight. Since this is completely opposite to the higher channels we will have a look at the source region.

The main precipitation of low energetic electrons (<1 keV) at daytime (e.g. 76–80 S, 6–13 MLT for TED electron band 4) most likely origins from the poleward edge of the cusp, referring to Sandholt et al. (1996); Øieroset et al. (1997); Sandholt et al. (2000) who attribute this as source region during periods with northward IMF (which in our study mostly refers to no-substorm periods as southward IMF triggers substorms).

In contrast, during periods with isolated substorms the precipitation particle flux is shifted by 2 degrees to the equator(the shift can be identified throughout TED electron bands 4 and 8). The source in this case is the equatorward edge of the cusp which has been identified as corresponding source region in periods of southward IMF by Sandholt and Newell (1992); Sandholt et al. (1998). A sketch including the source regions may be found in Newell and Meng (1992, Fig. 2), even though the regions are labled with Mantle and Cusp here.

Additionally it can be noticed that **noon sector electron fluxes decrease during a substorm**, which is clearly seen in all upper channels (from TED electron band 11 to mep0e2-e3).

An **increasing dusk-dawn asymmetry with substorm activity** (as e.g. Allison et al. (2017) noted for trapped radiation belt electrons) **cannot be identified**. In contrast, it seems that substorm activity simply adds particle precipitation in the night side and reduces high energetic electron precipitation around noonIn sum our findings support that high numbers of low energetic particles enter the magnetosphere preferentally on the front side through cusp and other boundary layers (Newell et al., 2009).

Proton flux in various channels in high latitudes on the southern hemisphere.

Figure 4 shows the same as Figure 3 but for protons . Comparing no-substorm periods (left panel) with isolated substorm periods (right panel) as well as with the electron precipitation from Figure 3, we can identify: The **protons also show an equatorward movement of the main precipitation zone with increasing particle energy**.

Low energetic protons Additionally low energetic protons (TED proton band 4–14) **show a second oval structure** show a second oval structure (approx. 50–65 S), which is associated with the drift loss cone (see the Section 3) and thus geographically localized near the SAA. The second oval structure itself is a artifact of the MLT-binning (see Fig. 1).

Quantitatively, the **proton particle precipitation shows distinct MLT dependence**,

4.2 Typical pattern in high energetic channels

The high electron channels (above >2 keV) show a displacement of the main particle flux with MLT from midnight (TED electron band 11) via morning sector (mep0e1-e2) to day sector (mep0e2-e3).

Concerning protons, between TED proton band 14 and the following channels (mep0P1 to mep0P3) the main particle flux shifts from midnight to the evening sector, which is oppositely directed to the electron displacement.

A potential explanation for the displacement in the higher electron channels (and the opposite directed shift of the protons) is the westward partial ring current in the night side which is closed by flied-aligned currents (Birkeland Region 2) into the ionosphere (Lockwood, 2013; Milan et al., 2017). While electrons in ring current drift eastwards and thus may precipitate predominantly in the morning sector, the protons undergo a westward drift and mainly precipitate in the evening sector. The energy dependence might be due to different drift velocities (Allison et al., 2017). A drift of electron precipitation (>20 keV) towards the dayside has also been reported by Matthews et al. (1988); Newell and Meng (1992); Østgaard et al. (1999) and is associated with central plasmasheet electron injections in the midnight region.

The resulting auroral asymmetry also depends on Kp-level, as shown in Section 4.3.

4.3 Kp-dependence of the auroral MLT-asymmetry

Even without Kp-dependence Figures 3 and 4 reveal a channel (energy) dependent MLT-asymmetry of the particle flux and that the range of this dependence changes with particle energy.

While e.g. the two lowest TED electron channels (band 4 and 8) show just minor MLT variations, it varies by more than one order of magnitude in the higher particle energies.

The proton flux shows distinct MLT dependence, ranging from just ~~**minor variations in TED proton band 11 and 14**~~ minor variations in TED proton band 11 and 14 (as well as ~~**no MLT variation in the highest MEPED channels**~~practically no MLT variation in the highest proton MEPED channels) up to about ~~**one order of magnitude in the lowest and medium particle energies**~~ one order of magnitude in the lowest and medium particle energies (TED proton band 4 and 8, MEPED mep0P1 and mep0P3).

During isolated substorms the maximum local time differences are similar or a factor of 2 higher~~(see Table **??**)~~.

~~In contrast to the electrons the **maximum asymmetry of protons does not depend on Kp-**~~index. However, we noticed that the MLT-asymmetry is not constant over different Kp-levels. This section will empahsis on the impact of Kp-levels using Figure 5, which is based on the auroral oval determination algorithm from Section 3.2 and presents the ratio between maximum and minimum auroral oval flux (or in other words the asymmetry of the oval) depending on Kp-level for every channel separately. Actually the channels have been grouped by their Kp dependency. All these findings are based on the whole period disregarding substorm or not.

~~Qualitatively: **Low energetic proton precipitation** (no-substorm) is **mostly concentrated around noon**. Additionally there is a slight increase from noon via the morning sector towards midnight.~~

The ~~precipitation **during isolated substorms is shifted to lower latitudes** by about~~ upper panel shows the 2 ~~degrees. Since we have seen a similar picture for low energetic electrons (see description to Figure 3, Paragraph **??**) we conclude that during no-substorm periods the particles originate from the poleward edge of the cusp , while during isolated substorms they originate from the equatorward edge of the cusp~~lowest electron channels and the lowest proton channel which all have a declining flux asymmetry with increasing Kp. The 6–6.7 Kp-bin is enhanced here, but we should keep in mind that this levels are occurring rarely and may suffer from bad statistics. A reason for the decline might be that the cusp inflow is not increasing with Kp as the rest of the auroral flux. Thus its relative fraction declines and subsequent declines the asymmetry.

The middle panel shows all particle channels that have an increasing flux asymmetry with Kp, as they are: all remaining electron channels and the proton channels TED band 11 and mep0P1. Given that high geomagnetic disturbance should be linked with enhanced acceleration, scattering and substorm processes increasing asymmetry in the affected regions suggests itself.

~~Between~~ The lowest panel gives the flux asymmetry dependencies of the remaining proton channels that are less distinct. It seems that there is a domain change at about 3.3 Kp since the asymmetry of TED proton band 14 and ~~the following channels (mep0P1 to~~ mep0P2 has a negative correlation below 3.3 and a positive one above. For the channels TED proton band 8 and mep0P3 ~~) the **main particle precipitation zone moves from midnight to the evening sector**, which is oppositely directed to the electron movement. The possible explanation has already been given in the description to Figure 3 (Paragraph 4.2).~~ the relationship is opposite.

~~The two **highest energy channels**~~

The two highest energy channels (MEPED mep0P4 and mep0P5) ~~**do not show MLT variations**~~do not show MLT variations as seen in Figure 4. Particle precipitation is limited to solar proton events. Since these particles enter the ionosphere via open field lines there is no latitudinal focussing but a homogeneous precipitation within the polar cap. Which is the reason why the auroral oval fit-routine failed and these channels are not listed in Fig. 5.

In sum, the maximum MLT-asymmetry depends on Kp:

- ~~Regarding the effect of **substorm** events, the **proton precipitation intensity at midnight sector outnumbers the no-substorm values** at the same place by factor 2 to 4.~~ for very low energy (proton and electron) it decreases with Kp,
- for higher electron channels it increases with Kp,
- for higher proton channels the Kp-dependence in ambiguous, but in general the asymmetry is significantly smaller than in the electron channels.

~~In contrast to the electron fluxes the **day sector proton fluxes do not significantly depend on substorm** activity.~~

4.4 Auroral oval asymmetry during substorms

This Section discusses the changes during substorm periods based on Figures 3, 4 and later on Fig. 6.

~~Exponent to the base 2 between lowest and highest flux in the auroral oval. Channel 0–1 1.3–2.3 2.7–9 no no no no sub proton band 4 4 3 3 3 3 proton band 8 3 3 3 3 3 proton band 11 1 1 2 1 2 proton band 14 1 1 1 1 2~~ In general, the particle flux during isolated substorms is similar to no-substorm periods, but superimposed with substorm-specific night-side (20–2 MLT) particle precipitation which reflects the substorm electrojet manifestations (Lockwood, 2013; Milan et al., 2017) (see Figures 3 and 4). In terms of particle acceleration this is the same region that shows Alfvén waves (compare Fig. 4 in Newell et al., 2009).

The electron and proton flux intensity at midnight sector outnumbers the no-substorm values at the same place by factor 2 to 4. For mep0P1 ~~3 3 3 4 5 mep0P2 4 4 4 4 5~~ to mep0P3 ~~2 3 3 3 4 mep0P4~~ also the evening sector is slightly increased during

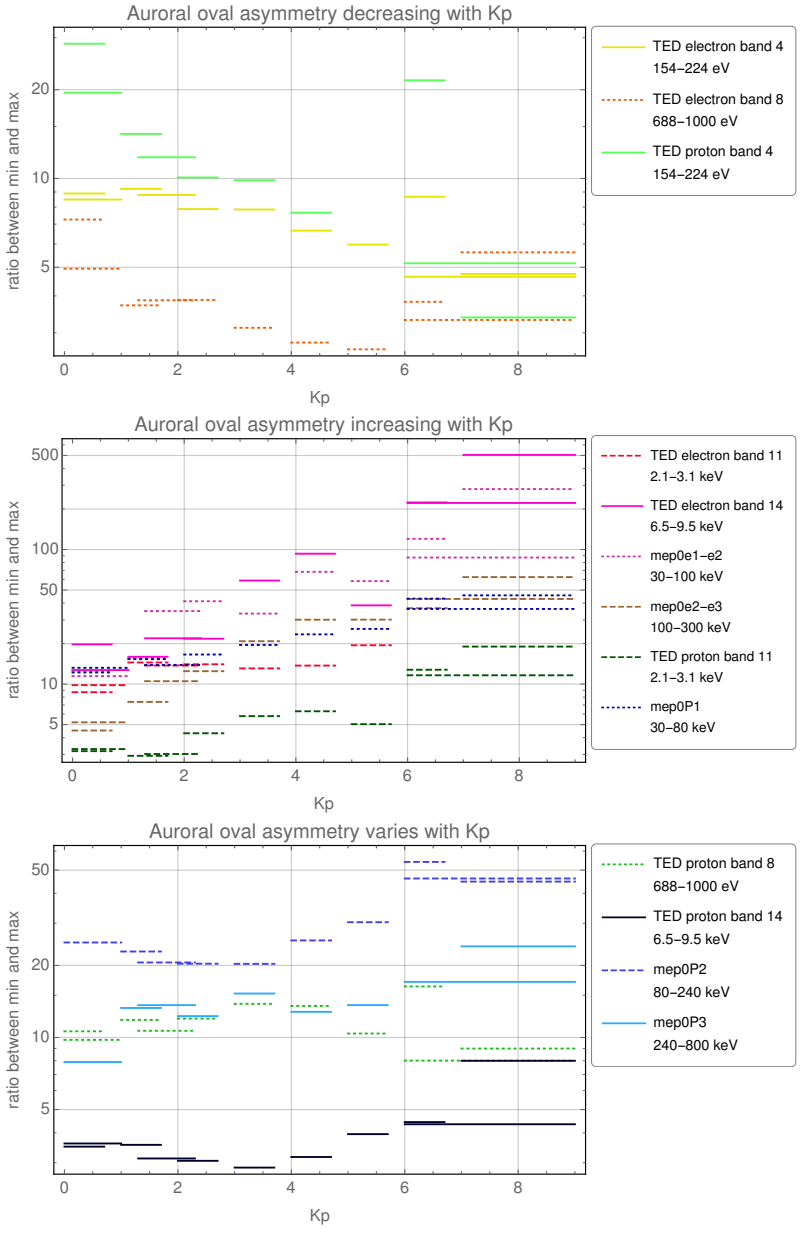

Figure 5. Dependence of the auroral oval asymmetry with Kp. Top: Channels which auroral oval flux shows a negative correlation with Kp, middle: positive correlation, bottom: no clear correlation.

substorms. Given the flux increase in the midnight sector the maximum auroral flux during a substorm can mostly be seen around 0~~0 0 0 1 mep0P5 0 0 0 0 0 1 electronband 4 3 3 2 2 2 electron band 8 2 1 1 1 2 electron band~~ MLT (see Figures 3 and 4).

Additionally noon sector electron fluxes decrease during a substorm, which is clearly seen in all upper channels (from TED electron band 11 ~~3 3 3 3 4 electron band 14 3 4 5 3 5 mep0e1-e2 3 4 5 5 5~~ to mep0e2-e3~~2 3 4 4 4~~

5 ~~Low Latitudes~~

~~Fig~~). The noon sector flux decreases most probably because dayside particle precipitation occurs often during northward orientated IMF which is not usual for substorms (see Figure 3). ~~1 (lower panel, 24°–52°N[1]) also revealed another obviously MLT-dependent pattern, which cannot be attributed to direct particle precipitation as in low latitudes the 0° (radially outward looking) detector measures particles that gyrate around their guiding field line with a high pitch angle. Thus we see a mostly trapped particle population here. Given that all Kp-bins show a similar MLT-pattern independently from substorm activity it seems worth mentioning – even though particle flux itself is small, not connected with precipitation and raising a couple of questions.~~

~~Figure ?? is a close-up of~~ In contrast to the ~~described region and shows particle flux in low latitudes in the Northern hemisphere. The northern hemisphere has been chosen to exclude the SAA.~~ electron fluxes the day-sector proton fluxes do not significantly depend on substorm activity (see Figures 4).

~~Our aim is to depict the MLT variations and how some of them might be explained.~~

~~Fig. ??~~ ~~reflects the limited local time coverage, even though up to five satellites have been used in an~~ Figure 6 presents how the asymmetry depends on substorms. Since an 8 ~~year period. The missing two local time bins from 23–1 h are marked in gray.~~

~~The color scale is logarithmic to a base of two, meaning the threshold to an adjacent colour is a factor of 2 apart. The reference value has been set individually for every channel to the lowest occurring value. Thus MLT differences can be easily identified and quantified. It should be noted that only~~ year period does not contain enough values for substorms in rare Kp-levels we neglected the Kp-level here and compared isolated substorm to no-substorm periods~~and just one of the probed Kp-levels is given here. The reason is that there is no distinct difference to substorm periods (except for worse statistics) and no significant difference to other Kp-levels as well.~~ .

~~Our findings are: **Typical for electron and proton TED bands is a flux minimum around midnight.** For the lowest channel,~~ Except for TED electron band 4 (where there is no significant difference between substorm and no-substorm periods) all other channels have an increased auroral oval asymmetry during isolated substorms. The numbers above and below the marked flux ratio indicate the MLT location of the minimum (below) and maximum (above). We can identify that the maximum flux during a substorm shifts to the midnight sector (if not already there in no-substorm periods) e.g. for mep0e1-e2, TED proton band 4 ~~(electron~~ and ~~proton), it is centered at midnight (20–4 MLT), for the higher TED channels it appears shifted to~~

[1] ~~Converting the modified APEX 110 km longitude into geographic longitude, the lower boundary is between 4.2 and 24.0° N while the upper boundary is between 39.6 and 55.8° N.~~

~~Relative particle flux in various channels in low latitudes on the Northern hemisphere in relation to the lowest occuring flux value. Gray~~

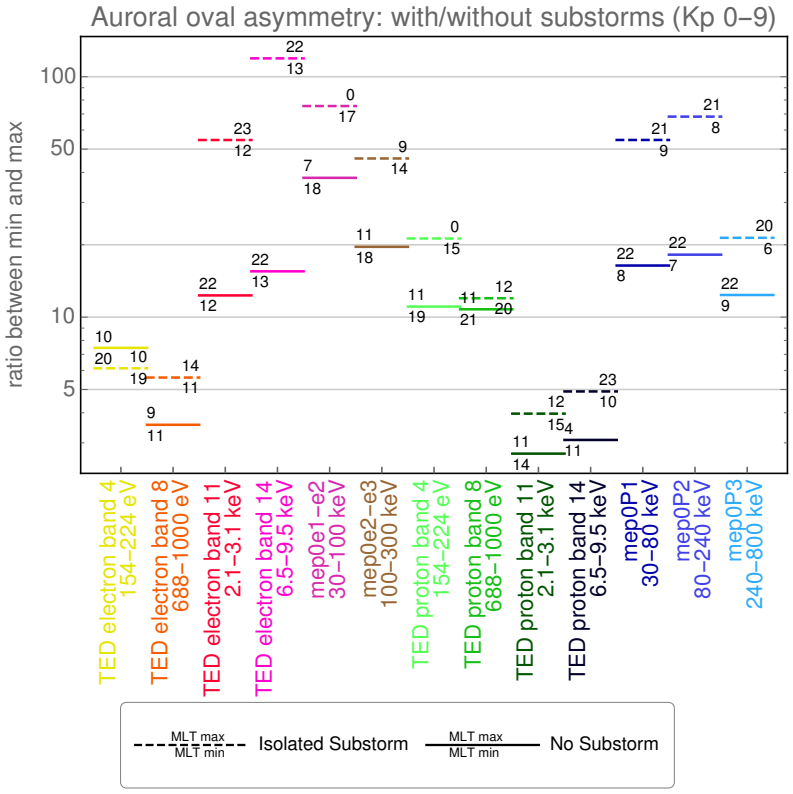

~~indicates missing data around midnight.~~

Figure 6. The auroral asymmetry is shown as reatio between maximum and minimum auroral oval flux. The number above a specific ratio states the MLT where the maximum is detected while the number below that ratio indicates the MLT of the minimum.

~~the morning sector centered around 2 or 3 MLT . While the general picture can be explained by the primary particle source being the sunlit ionosphere, which also justifies that the strongest day-night asymmetry is seen in the very low energetic channels, which are (or are close to) the thermal spectrum, the MLT-shift for higher energies remains unclear.~~ 14.

~~The **highest** electron (mep0e2-e3) and proton **channels** (mep0P2, mep0P3, mep0P4 and mep0P5)**do not show MLT-variations** in low latitudes. Since one reason for it has already been explained as these channels are far from the thermal source population another reason is given by Allison et al. (2017), who also investigated trapped electrons and explained the decreasing MLT-dependence with energy by higher drift velocity of high energetic particles that (in combination with closed drift paths) result in more uniform MLT patterns.~~

~~**At 14-16 MLT** however, **a local minimum can be found** in 5 channels (electron~~ For TED electron band ~~4,~~ 4 and 8 ~~and 14 and proton~~ (as well as TED proton band ~~11~~ 8 and ~~14) probably even in mep0P1, but then shifted by +2 MLT. The reason might be plasmaspheric plumes that are capable of transporting particles from the plasmasphere to the dusk sector of the dayside outer magnetosphere (**???**) and which often occur in this MLT range~~ 11) the substorm enhancement is also seen in the night

sector, but it does not overshoot the dayside flux (see Figures 3 and 4), while the substorm enhancement in the night-sector of mep0e2-e3 is in the same order as the 9–12 MLT flux.

This agrees with Newell et al. (2009) stating that the low energetic particles that enter the magnetosphere in the day-side are accelerated by the magnetotail and precipitating at the night-side during substorms.

Aspects that remain unclear but also can be identified in all Kp-bins are: **Medium** electron and proton **channel** (The asymmetry in both, the electron and the proton spectra (as well as during no-substorm or substorm periods) shows a local minimum in middle TED channels (TED electron band 8 and proton band 11) as well as a local maximum at higher energies (TED electron band 14 or mep0e1-e2 and for electron and mep0P1) **show a flux maximum around midnight** in contrast to the lower channels that have a local minimum here. It might also be that the midnight-minimum moved to the morning sector. However, the flux difference is just about a factor of 2 to 4, which is significantly less than in the low energetic channels or mep0P2 for protons). At even higher energies the asymmetry declines again.

A phenomena that can be identified in at least 6 channels (electron band

4.1 Latitudinal displacement of the maximum auroral flux depending on Kp and energy

Figure 7 presents how the latitude of the maximum auroral oval flux varies with particle energy and Kp. In advance we should note that Fig. 7 may not be over-iterpreted since latitudinal displacement of the maximum flux is mainly an effect of a MLT-shift (see Fig. 3) that causes the strong latitudinal change between TED electron band 8 , 11 and TED electron band 14 and for electrons and TED proton band 4, 11 and 14) is **a local flux maximum from 9-10 MLT**. It seems like a counter-part of the plasmaspheric plume since it is located in the same MLT distance to noon but on the morning sector . However, it is not known that something like a counter-part of the plasmaspheric plume exists. Consequently the reason for this flux enhancement is not known to the authors. mep0P1 for protons. Thus the main precipitation zone undergoes a strong latitudinal change, but it does not necessarily describe a latitudinal change in the auroral oval.

MLT flux difference at low latitudes. Maximum relative difference between flux measurements on the same latitude is presented. Please note that not ratio but its exponent to the base of two is given, meaning that the highest MLT-flux difference for protons (in proton band 8) is a factor $2^{11} = 2048$. Channel relative difference (exponent to 2^x) proton band

The figure has been derived by the auroral oval determination method discussed in Section 3.2 and displays the latitude of maximum auroral oval flux.

Except for some outliers, most of them belonging to TED proton band 4 during high Kp levels (> 6), the graphs show a clear equatorial dislocation with increasing energy. The 110 km APEX latitudinal range at a specific Kp-level is about 10° for electrons and 12-16° for protons. This dislocation however appears to be stepwise: TED electron band 4 and 8 are almost on the same latitude as well as TED electron band 14, mep0e1-e2 and mep0e2-e3 share the same latitude. For protons TED proton band 4proton band , 8 and 11 proton band 11 5 proton band 14 5 are almost on one latitude and the higher particle energies mep0P1 3 electron band and mep0P2 are co-located. This implies that these particles origin from the same souce population.

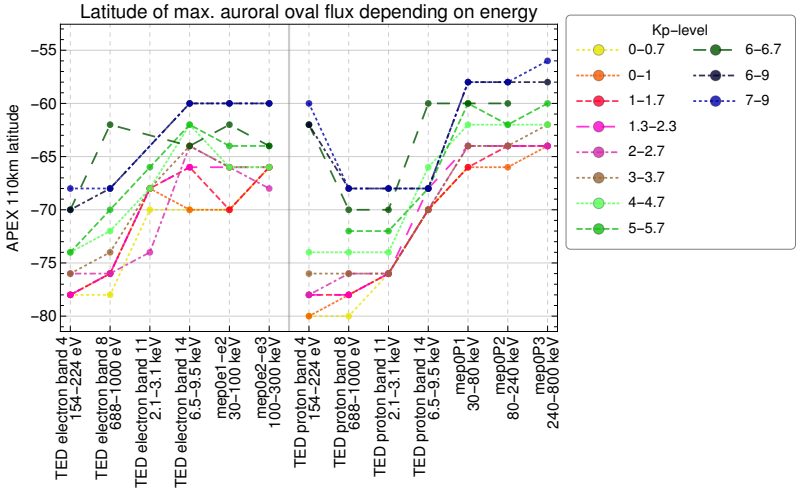

Figure 7. The modified APEX 110 km latitude of the maximum flux in the auroral oval is shown. Colors indicate specific Kp-levels. Left hand displays the energy dependence of electrons, right hand that one of the protons.

However, there is a noticable latitudinal shift with particle energy even for the particle channels that appear co-located. For 8 out of 11 Kp-levels there is an equatorial shift of 2° or more between TED electron band 4 and 8. For protons a latitudinal shift can be recognizend between TED proton band 4 and 11 ~~electron band~~ or between mep0P1 and mep0P3.

Every color graph represents the spectral location of the maximum flux latitude for a certain Kp-range. Thus we can infer that increased geomagnetic disturbance (high Kp values) causes a dislocation of up to about 8~~6 electron band 11~~ ° towards the equator.

Concerning the outliers in TED proton band 4~~electron band 14 6 mep0e1-e2 2~~ , for low Kp-values there is a clear flux maximum at noon, which is located at rather high latitudes (compare Fig. 3). At high Kp, the MLT asymmetry declines and then flips. Consequently the maximum flux for high Kp-levels is not in the day sector and thus at significantly lower latitudes, but even between the outliers and the maximum flux location in mep0P3 (which is in a similar MLT-region) we can recognize a latitudinal shift.

In sum, there is an equatorial shift of the main precipitation zone with increasing Kp and increasing particle energy, while the latter is primarily due to a shift in MLT and only secondarily due to a latitudinal shift of the auroral oval itself.

5 Summary

In this paper we presented the MLT-distribution of energetic particle flux/precipitation into the ionosphere in combination with different substorm activity~~as well as MLT-dependent trapped particle flux in the plasmasphere~~.

~~Concerning the precipitating particles we could identify different particle sources for low and high energetic particles . Different sources and energy-specific drifts lead to MLT-dependence of the dominating precipitation: < 1 keV in the day-sector~~

(protons concentrated at noon), above a few keV in the night-sector. Above that the charge-dependent drift clearly separates electron and proton precipitation. With increasing electron energy electrons move We could identify low energetic particles to predominantly precipitate around local noon, supporting the idea that they enter the magnetosphere through the cusp. During substorms the maximum particle flux is shifted by 2 degrees to the equator.

Higher particles energies show a different behavior. Electrons (>2 keV) mainly precipitate at midnight but with increasing particle energy the maximum flux shifts via morning-sector to the day-sector, while the main proton precipitation moves to the evening sector with a maximum at about 22 MLT. Maximum protons flux on the other hand, shift from the midnight-sector to the evening-sector with increasing energy. A drift of electron precipitation (>20 keV) towards the dayside is associated with central plasmasheet electron injections in the midnight region.

Also quantitatively the MLT-variation depends on energy : with a few 100 eV the relatively focussed peak at noon produces a medium asymmetry (exponent 2–3). With slightly higher energies that vanishes and the asymmetry declines (exponent 1–2) . As soon as the (partial)ring current becomes dominant the asymmetry peaks (exponent up to 5). For higher energies (just protons available) the asymmetry breaks down to zero.

While the MLT-variation is invariant in Kp for protons, the MLT-asymmetry for electrons depends on geomagnetic disturbance. There is an energy dependend auroral asymmetry. While the low energetic electrons have just a minor asymmetry it enhances to more than one order of magnitude for the higher electron channels. For low energetic protons the cusp precipitation causes an asymmetry of about an order of magnitude. Above that energy the asymmetry first declines (to factor 2 in TED proton band 11 and 14) and than enlarges again with the MEPED channels 1 to 3 (more than an order of magnitude). For highest proton channels the asymmetry disappears as these particles are not linked with auroral precipitation. During substorms the maximum flux is similar or a factor 2 higher.

The auroral asymmetry is Kp-dependend. For low energetic electrons $<$ 1 keV it particles the asymmety declines with Kp and for electron $>$ 6 keV it increases with Kp.

The effect of substorms is mostly limited to the night-sector, where it generally enhances particle precipitation . For electrons the day-sector also is affected, where electron precipitation declines (seen for 2–300 keV) probably due to lack of cusp precipitation during high Kp-values, while it increases especially (stronger) for higher electron channels probably due to increased acceleration and scattering processes. For medium energy protons (30–800 keV) the evening sector is slightly increased. Quantitatively, isolated-substorm periods enhance the flux in the night sector by approx. factor 2 to 4, while the day-sector decrease might be up to factor 2. Consequently the resulting MLT-differences enlarge during substorms. and high energetic protons the development of the asymmetry with Kp is not that distinct, there might be multiple processes involved.

MLT-dependency at low latitudes are regarded even though they are not linked to particle precipitation, but because they show a) extreme asymmetries (up to a ratio of 1:2000), which can be attibuted to the particle source of the plasmasphere, being the sunlit thermosphere and b) because one MLT-region shows a depletion which might be due to a plasmaspheric plume. However, some of the MLT-features at low latitudes still raise questionsDuring substorms the no-substorm flux seems to be generally superimposed by substorm-specific night-side particle flux. However, the noon-sector fluxes depend on particle species. For protons they seem to be independed from substorm activity, while for electrons they decrease during a substorm.

Also we noticed a Kp and energy dependend equatorial shift of the main flux latitude.

Competing interests. The authors declare that they have no conflict of interest.

Acknowledgements. The authors acknowledge the NOAA National Centers for Environmental Information (https://ngdc.noaa.gov/stp/satellite/poes/dataaccess.html) for the POES and METOP particle data used in this study and give many thanks to the SuperMAG team (http://supermag.jhuapl.edu/) and their collaborators (http://supermag.jhuapl.edu/info/?page=acknowledgement).
The work is supported by the DFG project WI4417/2-1.

References

Akasofu, S.-I.: The development of the auroral substorm, Planet. Space Sci., 12, 273–282, https://doi.org/10.1016/0032-0633(64)90151-5, 1964.

Akasofu, S.-I.: Auroral substorms as an electrical discharge phenomenon, Progress in Earth and Planetary Science, 2, 20, https://doi.org/10.1186/s40645-015-0050-9, 2015.

Akasofu, S. I., Chapman, S., and Meng, C. I.: The polar electrojet, Journal of Atmospheric and Terrestrial Physics, 27, 1275–1300, https://doi.org/10.1016/0021-9169(65)90087-5, 1965.

Allison, H. J., Horne, R. B., Glauert, S. A., and G., D.: The magnetic local time distribution of energetic electrons in the radiation belt region, J. Geophys. Res. Space Physics, 122, 20, https://doi.org/doi:10.1002/2017JA024084, 2017.

Asikainen, T., Mursula, K., and Maliniemi, V.: Correction of detector noise and recalibration of NOAA/MEPED energetic proton fluxes, J. Geophys. Res., 117, A09 204, https://doi.org/doi:10.1029/2012JA017593, 2012.

Bartels, J., Heck, N. H., and Johnston, H. F.: The three-hour-range index measuring geomagnetic activity, Terrestrial Magnetism and Atmospheric Electricity, 1939.

Berkey, F. T., Driatskiy, V. M., Henriksen, K., Hultqvist, B., Jelly, D. H., Shchuka, T. I., Theander, A., and Ylindemi, J.: A synoptic investigation of particle precipitation dynamics for 60 substorms in IQSY (1964-1965) and IASY (1969), Planetary and Space Science, 22, 255–307, https://doi.org/10.1016/0032-0633(74)90028-2, 1974.

Birn, J., Thomsen, M. F., Borovsky, J. E., Reeves, G. D., McComas, D. J., and Belian, R. D.: Characteristic plasma properties during dispersionless substorm injections at geosynchronous orbit, J. Geophys. Res., 102, 2309–2324, https://doi.org/10.1029/96JA02870, 1997. ~~Borovsky~~

Bornebusch, J. ~~E., Denton, M. H., Denton, R. E., Jordanova, V. K., and Krall, ~~, Wissing, J.~~: Estimating the effects of ionospheric plasma on solar wind/magnetosphere coupling via mass loading of dayside reconnection: Ion-plasma-sheet oxygen, plasmaspheric drainage plumes, and the plasma cloak, Journal of Geophysical Research: Space Physics, 118, 5695–5719, ~~, and Kallenrode, M.-B.: Solar particle precipitation into the polar atmosphere and their dependence on hemisphere and local time, Advances in Space Research, 45, 632 – 637, https://doi.org/https://doi.org/10.1016/j.asr.2009.11.008, ~~, 2013. ~~http://www.sciencedirect.com/science/article/pii/S027311770900711X, 2010.

Callis, L. B., Baker, D. N., Natarajan, M., Bernard, J. B., Mewaldt, R. A., Selesnick, R. S., and Cummings, J. R.: A 2-D model simulation of downward transport of NO_y into the stratosphere: Effects on the 1994 austral spring $O_3$and NO_y, Geophys. Res. Lett., 23, 1905–1908, https://doi.org/10.1029/96GL01788, 1996a.

Callis, L. B., Boughner, R. E., Baker, D. N., Mewaldt, R. A., Bernard Blake, J., Selesnick, R. S., Cummings, J. R., Natarajan, M., Mason, G. M., and Mazur, J. E.: Precipitating electrons: Evidence for effects on mesospheric odd nitrogen, Geophys. Res. Lett., 23, 1901–1904, https://doi.org/10.1029/96GL01787, 1996b.

~~Chen, S.-H. and Moore, ~~

Davis, T. ~~E.~~ N. and Sugiura, M.: ~~Magnetospheric convection and thermal ions in the dayside outer magnetosphere~~Auroral electrojet activity index AE and its universal time variations, J. Geophys. Res., 71, 785–801, https://doi.org/10.1029/JZ071i003p00785, 1966.

Dombeck, J., Cattell, C., Prasad, N., Meeker, E., Hanson, E., and McFadden, J.: Identification of Auroral Electron Precipitation Mechanism Combinations and Their Relationships to Net Downgoing Energy and Number Flux, Journal of Geophysical Research ~~: Space Physics, 111, , , 2006. ~~(Space Physics), 123, 10, https://doi.org/10.1029/2018JA025749, 2018.

Evans, D. S. and Greer, M. S.: Polar Orbiting Environmental Satellite Space Environment Monitor - 2, Instrument Descriptions and Archive Data Documentation, National Oceanic and Atmospheric Administration, NOAA Space Environ. Lab, Boulder, Colorado, USA, version 1.4b, including TED calibrations, 2004.

Evans, D. S. and Greer, M. S.: Polar Orbiting Environmental Satellite Space Environment Monitor - 2, Instrument Descriptions and Archive Data Documentation, National Oceanic and Atmospheric Administration, NOAA Space Environ. Lab, Boulder, ~~Colo~~Colorado, USA, version 2.0, 2006.

Frank, L. A., Craven, J. D., Ackerson, K. L., English, M. R., Eather, R. H., and Carovillano, R. L.: Global auroral imaging instrumentation for the Dynamics Explorer Mission, Space Science Instrumentation, 5, 369–393, 1981.

Fujii, R., Hoffman, R. A., Anderson, P. C., Craven, J. D., Sugiura, M., Frank, L. A., and Maynard, N. C.: Electrodynamic parameters in the nighttime sector during auroral substorms, J. Geophys. Res., 99, 6093–6112, https://doi.org/10.1029/93JA02210, 1994.

Gjerloev, J., Hoffman, R., Friel, M., Frank, L., and Sigwarth, J.: Substorm behavior of the auroral electrojet indices, Annales Geophysicae, 22, 2135–2149, https://doi.org/10.5194/angeo-22-2135-2004, 2004.

Hardy, D. A., Gussenhoven, M. S., and Holeman, E.: A statistical model of auroral electron precipitation, J. Geophys. Res., 90, 4229–4248, https://doi.org/10.1029/JA090iA05p04229, 1985.

Heath, D. F., Krueger, A. J., and Crutzen, P. J.: Solar proton event - Influence on stratospheric ozone, Science, 197, 886–889, https://doi.org/10.1126/science.197.4306.886, 1977.

Lockwood, M.: Reconstruction and Prediction of Variations in the Open Solar Magnetic Flux and Interplanetary Conditions, Living Reviews in Solar Physics, 10, 4, https://doi.org/10.12942/lrsp-2013-4, 2013.

Logachev, Y. I., Bazilevskaya, G. A., Vashenyuk, E. V., Daibog, E. I., Ishkov, V. N., Lazutin, L. L., Miroshnichenko, L. I., Nazarova, M. N., Petrenko, I. E., Stupishin, A. G., Surova, G. M., and Yakovchuk, O. S.: Catalog of solar proton events in the 23rd cycle of solar activity (1996-2008), 2016.

Matthews, D. L., Rosenberg, T. J., Benbrook, J. R., and Bering, III, E. A.: Dayside energetic electron precipitation over the South Pole (lambda = 75 deg), Journal of Geophysical Research, 93, 12 941–12 945, https://doi.org/10.1029/JA093iA11p12941, 1988.

McPherron, R. L.: Growth phase of magnetospheric substorms, J. Geophys. Res., 75, 5592, https://doi.org/10.1029/JA075i028p05592, 1970.

Mende, S. B., Frey, H. U., Morsony, B. J., and Immel, T. J.: Statistical behavior of proton and electron auroras during substorms, Journal of Geophysical Research (Space Physics), 108, 1339, https://doi.org/10.1029/2002JA009751, 2003.

Meredith, N. P., Horne, R. B., Lam, M. M., Denton, M. H., Borovsky, J. E., and Green, J. C.: Energetic electron precipitation during high-speed solar wind stream driven storms, Journal of Geophysical Research (Space Physics), 116, A05223, https://doi.org/10.1029/2010JA016293, 2011.

Milan, S. E., Clausen, L. B. N., Coxon, J. C., Carter, J. A., Walach, M.-T., Laundal, K., Østgaard, N., Tenfjord, P., Reistad, J., Snekvik, K., Korth, H., and Anderson, B. J.: Overview of Solar Wind-Magnetosphere-Ionosphere-Atmosphere Coupling and the Generation of Magnetospheric Currents, Space Science Rev., 206, 547–573, https://doi.org/10.1007/s11214-017-0333-0, 2017.

Newell, P. T. and Gjerloev, J. W.: Evaluation of SuperMAG auroral electrojet indices as indicators of substorms and auroral power, Journal of Geophysical Research (Space Physics), 116, A12211, https://doi.org/10.1029/2011JA016779, 2011a.

Newell, P. T. and Gjerloev, J. W.: Substorm and magnetosphere characteristic scales inferred from the SuperMAG auroral electrojet indices, Journal of Geophysical Research (Space Physics), 116, A12232, https://doi.org/10.1029/2011JA016936, 2011b.

Newell, P. T. and Meng, C.-I.: Mapping the dayside ionosphere to the magnetosphere according to particle precipitation characteristics, Journal of Geophysical Research, 19, 609–612, https://doi.org/10.1029/92GL00404, 1992.

Newell, P. T., Sotirelis, T., and Wing, S.: Diffuse, monoenergetic, and broadband aurora: The global precipitation budget, Journal of Geophysical Research: Space Physics, 114, https://doi.org/10.1029/2009JA014326, https://agupubs.onlinelibrary.wiley.com/doi/abs/10.1029/2009JA014326, 2009.

Newell, P. T., Lee, A. R., Liou, K., Ohtani, S.-I., Sotirelis, T., and Wing, S.: Substorm cycle dependence of various types of aurora, Journal of Geophysical Research: Space Physics, 115, https://doi.org/10.1029/2010JA015331, https://agupubs.onlinelibrary.wiley.com/doi/abs/10.1029/2010JA015331, 2010.

Øieroset, M., Sandholt, P. E., Denig, W. F., and Cowley, S. W. H.: Northward interplanetary magnetic field cusp aurora and high-latitude magnetopause reconnection, Journal of Geophysical Research, 102, 11 349–11 362, https://doi.org/10.1029/97JA00559, 1997.

Østgaard, N., Stadsnes, J., Bjordal, J., Vondrak, R. R., Cummer, S. A., Chenette, D. L., Parks, G. K., Brittnacher, M. J., and McKenzie, D. L.: Global-scale electron precipitation features seen in UV and X rays during substorms, Journal of Geophysical Research, 104, 10 191–10 204, https://doi.org/10.1029/1999JA900004, 1999.

Reeves, G. D., Henderson, M. G., Skoug, R. M., Thomsen, M. F., Borovsky, J. E., Funsten, H. O., C:son Brandt, P., Mitchell, D. J., Jahn, J.-M., Pollock, C. J., McComas, D. J., and Mende, S. B.: IMAGE, POLAR, and Geosynchronous Observations of Substorm and Ring Current Ion Injection, in: Disturbances in Geospace: The Storm-substorm Relationship, edited by Surjalal Sharma, A., Kamide, Y., and Lakhina, G. S., vol. 142 of *Washington DC American Geophysical Union Geophysical Monograph Series*, p. 91, https://doi.org/10.1029/142GM09, 2003.

Richmond, A. D.: Ionospheric Electrodynamics Using Magnetic Apex Coordinates., Journal of Geomagnetism and Geoelectricity, 47, 191–212, https://doi.org/10.5636/jgg.47.191, 1995.

Rodger, C. J., Clilverd, M. A., Green, J. C., and Lam, M. M.: Use of POES SEM-2 observations to examine radiation belt dynamics and energetic electron precipitation into the atmosphere, Journal of Geophysical Research: Space Physics, 115, https://doi.org/10.1029/2008JA014023, https://agupubs.onlinelibrary.wiley.com/doi/abs/10.1029/2008JA014023, 2010.

Sandholt, P. E. and Newell, P. T.: Ground and satellite observations of an auroral event at the cusp/cleft equatorward boundary, Journal of Geophysical Research, 97, 8685–8691, https://doi.org/10.1029/91JA02995, 1992.

Sandholt, P. E., Farrugia, C. J., Øieroset, M., Stauning, P., and Cowley, S. W. H.: Auroral signature of lobe reconnection, Geophysical Research Letters, 23, 1725–1728, https://doi.org/10.1029/96GL01846, 1996.

Sandholt, P. E., Farrugia, C. J., Moen, J., and Cowley, S. W. H.: Dayside auroral configurations: Responses to southward and northward rotations of the interplanetary magnetic field, Journal of Geophysical Research, 103, 20 279–20 296, https://doi.org/10.1029/98JA01541, 1998.

Sandholt, P. E., Farrugia, C. J., Cowley, S. W. H., Lester, M., Denig, W. F., Cerisier, J.-C., Milan, S. E., Moen, J., Trondsen, E., and Lybekk, B.: Dynamic cusp aurora and associated pulsed reverse convection during northward interplanetary magnetic field, Journal of Geophysical Research, 105, 12 869–12 894, https://doi.org/10.1029/2000JA900025, 2000.

Thorne, R. M.: Energetic radiation belt electron precipitation - A natural depletion mechanism for stratospheric ozone, Science, 195, 287–289, https://doi.org/10.1126/science.195.4275.287, 1977.

~~Walsh, A. P., Haaland, S., Forsyth, C., Keesee, A. M., Kissinger, J., Li, K., Runov, A., Soucek, J., Walsh, B. M., Wing, S., and Taylor, M. G. G. T.: Dawn–dusk asymmetries in the coupled solar wind–magnetosphere–ionosphere system: a review, Annales Geophysicae, 32, 705–737, , , 2014.~~

Wissing, J. M., Bornebusch, J., and Kallenrode, M.-B.: Variation of energetic particle precipitation with local magnetic time, Advances in Space Research, 41, 1274–1278, https://doi.org/10.1016/j.asr.2007.05.063, 2008.

Yando, K., Millan, R. M., Green, J. C., and Evans, D. S.: A Monte Carlo simulation of the NOAA POES Medium Energy Proton and Electron Detector instrument, Journal of Geophysical Research: Space Physics, 116, https://doi.org/10.1029/2011JA016671, https://agupubs.onlinelibrary.wiley.com/doi/abs/10.1029/2011JA016671, 2011.